(2)

NAVAL POSTGRADUATE SCHOOL

Monterey, California

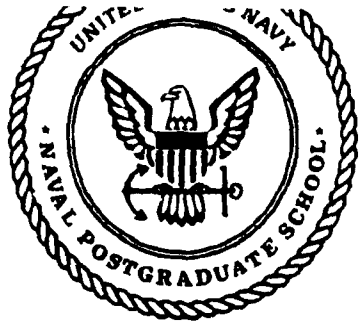

Original contains color plates: All DTIC reproductions will be in black and white

THESIS

COMPARISON OF AREAL EXTENT OF
SNOW AS DETERMINED BY
AVHRR AND SSM/I SATELLITE IMAGERY

by

Robert W. Maxson

September, 1992

Thesis Advisor: Philip A. Durkee

Approved for public release; distribution is unlimited

DISCLAIMER NOTICE

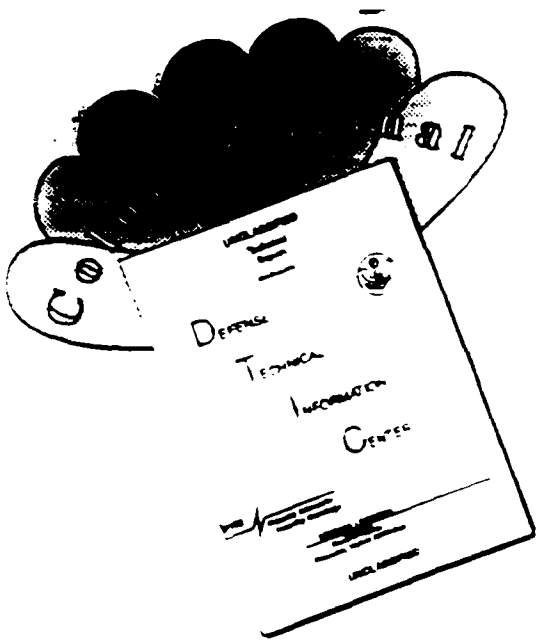

THIS DOCUMENT IS BEST QUALITY AVAILABLE. THE COPY FURNISHED TO DTIC CONTAINED A SIGNIFICANT NUMBER OF COLOR PAGES WHICH DO NOT REPRODUCE LEGIBLY ON BLACK AND WHITE MICROFICHE.

REPORT DOCUMENTATION PAGE

1a. REPORT SECURITY CLASSIFICATION UNCLASSIFIED	1b RESTRICTIVE MARKINGS
2a. SECURITY CLASSIFICATION AUTHORITY	3 DISTRIBUTION/AVAILABILITY OF REPORT Approved for public release; distribution is unlimited.
2b. DECLASSIFICATION/DOWNGRADING SCHEDULE	
4. PERFORMING ORGANIZATION REPORT NUMBER(S)	5. MONITORING ORGANIZATION REPORT NUMBER(S)
6a. NAME OF PERFORMING ORGANIZATION Naval Postgraduate School 6b. OFFICE SYMBOL (*If applicable*) 35	7a. NAME OF MONITORING ORGANIZATION Naval Postgraduate School
6c. ADDRESS (*City, State, and ZIP Code*) Monterey, CA 93943-5000	7b. ADDRESS (*City, State, and ZIP Code*) Monterey, CA 93943-5000
8a. NAME OF FUNDING/SPONSORING ORGANIZATION 8b. OFFICE SYMBOL (*If applicable*)	9. PROCUREMENT INSTRUMENT IDENTIFICATION NUMBER
8c. ADDRESS (*City, State, and ZIP Code*)	10. SOURCE OF FUNDING NUMBERS Program Element No. / Project No. / Task No. / Work Unit Accession Number

11. TITLE (*Include Security Classification*)
COMPARISON OF AREAL EXTENT OF SNOW AS DETERMINED BY AVHRR AND SSM/I SATELLITE IMAGERY

12. PERSONAL AUTHOR(S) Robert W. Maxson

13a. TYPE OF REPORT	13b. TIME COVERED	14. DATE OF REPORT (*year, month, day*)	15. PAGE COUNT
Master's Thesis	From To	September, 1992	106

16. SUPPLEMENTARY NOTATION
The views expressed in this thesis are those of the author and do not reflect the official policy or position of the Department of Defense or the U.S. Government.

17. COSATI CODES			18. SUBJECT TERMS (*continue on reverse if necessary and identify by block number*)
FIELD	GROUP	SUBGROUP	AVHRR, imagery, satellite, SSM/I, snow

19. ABSTRACT (*continue on reverse if necessary and identify by block number*)

Advanced Very High Radiometric (AVHRR) and Special Sensor Microwave Imager (SSM/I) imagery are compared to determine the areal extent of snow. A multi-spectral AVHRR algorithm, utilizing channels 1 (0.63um), 2 (0.87 um), 3 (3.7um), and 4 (11.0um), creates a synthetic image that classifies land, snow, water and clouds. The classified images created by this algorithm serve as a baseline for a second algorithm that examines spatially and temporally matched SSM/I imagery. The SSM/I separation algorithm uses the 85 GHz horizontally polarized channel as well as the 37 GHz horizontally and vertically polarized channels. The synthetic image created by this algorithm classifies land, snow and water. Both separation algorithms use empirically derived separation thresholds obtained from bi-spectral scatter plots. Separation is made at a given pixel location based on the radiative identity assigned to that location from various wavelength combinations. The AVHRR data provides high resolution, daytime images of the snow pack but is completely dependent on the absence of clouds to view this ground based feature. The SSM/I data gives lower resolution imagery of the snow during daylight or night time satellite passes and is not affected by the presence of non-precipitating clouds. A total of 12 sub scenes are analyzed using both data sets and general agreement of the two sets of imagery is established.

20. DISTRIBUTION/AVAILABILITY OF ABSTRACT	21. ABSTRACT SECURITY CLASSIFICATION	
☐ UNCLASSIFIED/UNLIMITED ☐ SAME AS REPORT ☐ DTIC USERS	UNCLASSIFIED	
22a. NAME OF RESPONSIBLE INDIVIDUAL Philip A. Durkee	22b. TELEPHONE (*Include Area code*) 408-646-3465	22c. OFFICE SYMBOL MR/De

DD FORM 1473, 84 MAR 83 APR edition may be used until exhausted
All other editions are obsolete

Approved for public release; distribution is unlimited.

Comparison of Areal Extent of Snow as Determined by
AVHRR and SSM/I Satellite Imagery
by

Robert W. Maxson
Lieutenant Commander, National Oceanic and Atmospheric Administration
B.S., Florida Institute of Technology, 1978

Submitted in partial fulfillment
of the requirements for the degree of

MASTER OF SCIENCE IN METEOROLGY AND PHYSICAL OCEANOGRAPHY

from the

NAVAL POSTGRADUATE SCHOOL
September, 1992

Author: _____
Robert W. Maxson

Approved by: _____
Philip A. Durkee, Thesis Advisor

_____
Carlyle H. Wash, Second Reader

_____
Robert L. Haney, Chairman
Department of Meteorolgy

ABSTRACT

Advanced Very High Resolution Radiometric (AVHRR) and Special Sensor Microwave Imager (SSM/I) imagery are compared to determine the areal extent of snow. A multi-spectral AVHRR algorithm, utilizing channels 1 ($0.63\,\mu\,m$), 2 ($0.87\,\mu\,m$), 3 ($3.7\,\mu\,m$) and 4 ($11.0\,\mu\,m$), creates a synthetic image that classifies land, snow, water and clouds. The classified images created by this algorithm serve as a baseline for a second algorithm that examines spatially and temporally matched SSM/I imagery. The SSM/I separation algorithm uses the 85 GHz horizontally polarized channel as well as the 37 GHz horizontally and vertically polarized channels. The synthetic image created by this algorithm classifies land, snow and water. Both separation algorithms use empirically derived separation thresholds obtained from bi-spectral scatter plots. Separation is made at a given pixel location based on the radiative identity assigned to that location from various wavelength combinations. The AVHRR data provides high resolution, daytime images of the snow pack but is completely dependent on the absence of clouds to view this ground based feature. The SSM/I data gives lower resolution imagery of the snow during daylight or night time satellite passes and is not affected by the presence of non-precipitating clouds. A total of 12 sub scenes are analyzed using both data sets and general agreement of the two sets of imagery is established.

TABLE OF CONTENTS

ACKNOWLEDGMENTS

I would like to thank the NOAA Corps, specifically Admiral R.L. Speer (RET.) and Admiral E.D. Moran, for giving me the opportunity to come to the Naval Postgraduate School. The road through this curriculum is both challenging and rewarding. I will be able to apply the knowledge gained here to further the NOAA mission.

I am deeply indebted to the outstanding faculty of the Meteorology and Oceanography Departments who took someone who had been out of school for 12 years and made him academically competitive in two years. They were always approachable and helpful as well as being superior instructors. I don't take this gift lightly.

I had a great deal of help with this thesis. Dr. P.A. Durkee, my advisor, allowed me to pick a topic beneficial to an active NOAA program and guided me along the way. Dr. C.H. Wash, my reader, helped pull this whole project together. Dr. T.R. Carroll, NOAA graciously provided the AVHRR CD-ROMs and Dr. R.L. Armstrong, CIRES/NSIDC sent me the elusive SSM/I data. Mr. C.E. Motell wrote the software that allowed the AVHRR CD-ROM images to be brought into the VAX computer while Mr. C.E. Skupniewicz imaged the SSM/I data into the VAX.

I constantly received encouragement and help from my curricular officer, Commander T.K. Cummings, USN as well as academic assistance from my friend Lieutenant Commander (SEL.) T.D. Tisch, NOAA. Additional support was always available from Captain K.J. Schnebele, NOAA and Commander D.L. Gardner, NOAA who were the NPS-NOAA liaison officers.

I am extremely grateful to my beautiful wife Missy who keeps it all going, not only in Monterey but elsewhere, especially when I'm at sea or on permanent TDY. Finally, thanks to my daughters, Leigh and Katelyn, who regardless of the consequences of the past day, always make me feel special when I come home.

I. INTRODUCTION

A. BACKGROUND

Measurement of areal extent of snow cover has long been of interest to hydrologists and has more recently been considered for assessment of long term changing global climate. Over short time scales, significant snow fall followed by quickly rising above freezing temperatures can result in river flooding conditions that can threaten life and property. Intermediate to long range forecasts predict the water available from the seasonal snow melt and allow state and federal water resource management programs to determine the best plan of water distribution. At the climatic scale, significant increase or decrease in the areal extent of snow fall with its attendant seasonal change in planetary albedo may be an expression of changing climate.

The arrival of global satellite coverage of the earth has allowed large scale measurements of the snow pack to be completed on a near real time basis for both scientific research and operational hydrological prediction. Daily overhead passes are available from National Oceanic and Atmospheric (NOAA) satellites as well as from other spacecraft, such as the Defense Meteorological Space Program (DMSP) satellites. The NOAA satellites fly sensors, the Advanced Very High Resolution Radiometric (AVHRR), that are capable of viewing the earth in visible through infrared wavelengths while the DMSP platforms also include passive microwave wavelengths.

Figure 1.1 is an example of an AVHRR image as viewed in the channel 1 using visible wavelengths. This is a daytime image from the NOAA-11 orbiter as viewed on 20 February 1990, over the Great Lakes region of the United States. In this scene snow clearly covers the ground around the north and south sides of Lake Ontario and extends

along the St. Lawrence River to the Northeast. The dense Adirondack Forest is an oval shaped area that is positioned between Lake Champlain and Lake Ontario. The conifer trees in this region make it difficult to determine if snow is on the ground in the forest. This is also true in the Canadian forests to the north of the lake. Although the scene is nearly cloud free, some cumulus type clouds can be seen moving southeast from the southern side of Lake Ontario.

Figure 1.1- AVHRR channel 1 image of upstate New York on 20 February 1990.

Interpretation of images produced from the radiometric data from these satellites and the correct classification of viewed surfaces such as cloud overlying snow has been investigated recently by Allen (1987), Allen *et al* (1990), and Barron (1988). These studies concentrated on the separation of clouds from underlying snow and determined cloud cover from satellites in winter environments for tactical reasons. While the focus of these papers was more interested in the nature and extent of cloud cover as opposed to the extent of the snow cover itself, a great deal of progress was made in the ability to use automated multispectral techniques to classify satellite AVHRR images.

Other studies have examined the properties of the snow pack as viewed using passive microwave imagery. McFarland *et al* (1987) studied snow properties as observed in microwave images and were able to detect the edge of the snow pack by using the 37 GHz temperature polarization difference. Knuzi *et al* (1982) and Ferraro *et al* (1986) were able to discern the snow pack from snow free land by using multichannel temperature difference techniques. Regardless of method, the potential for observing the snow pack from space using passive microwave data has been well established.

Figure 1.2 shows the Great Lakes region of the United States as imaged by the DMSP Special Sensor Microwave/ Imager (SSM/I) on 20 February 1990. This image covers the same location as Figure 1.1 using the 85 GHz horizontally polarized channel. Compared to the AVHRR image a loss of resolution is immediately noted. Lake Ontario is well defined but Lake Champlain has been reduced to six clustered pixels. The Adirondack Forest area is again noticeable as an oval shaped region. Locations of definite snow cover in the AVHRR image are a darker gray in the SSM/I image due to the scattering effect of the overlying snow. The snow line appears discernible in the SSM/I image.

Both AVHRR and SSM/I imagery have strengths and weaknesses when used to observe the snow field. AVHRR data offers approximately one km resolution of the earth's surface when the satellite is viewing at nadir but the success of seeing the ground is totally dependent on the absence of clouds. SSM/I imagery is nearly independent of atmospheric conditions but its best resolution is approximately 14 km when the 85 GHz channel is used.

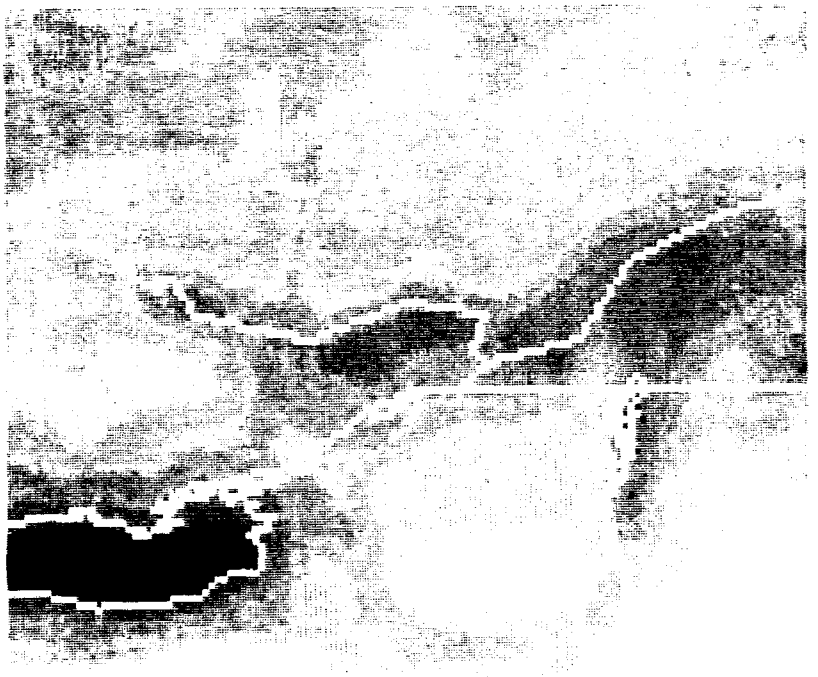

Figure 1.2 - SSM/I 85 GHz horizontally polarized image of upstate New York on 20 February 1990.

B. MOTIVATION

The National Oceanic and Atmospheric Administration operates the National Operational Hydrologic Remote Sensing Center (NOHRSC) as part of the National Weather Service (NWS). This center uses remotely sensed data to produce a variety of products necessary to support the hydrological missions of the NWS. In conjunction with airborne generated data sets, data from satellites are used to issue river and flood forecasts as well as to support national water resource management efforts.

Knowledge of the location and the extent of snow cover in North America is of vital importance to NOHRSC so that secondary, more exact survey of the snow pack can be accomplished. Actual snow water equivalent of the snow is obtained throughout the United States and Canada from low level aircraft measurements. Accurate satellite analysis of areal extent of snow cover on a near real time basis allows the NOHRSC to utilize its equipment and personnel in the most efficient manner as well as to provide more accurate snow pack estimates to the NWS.

Validation and improvements of existing AVHRR image classification techniques will have tangible benefit to the NOHRSC which must accomplish research during time frames that do not interfere with a busy operational mission. The addition of microwave channels into the study will also provide the NOHRSC with an initial feasibility study that will examine the usefulness of this type of data in an operational format.

C. OBJECTIVES

The central focus of this thesis is how to best determine the areal extent of snow cover using both AVHRR and SSM/I imagery. The radiative signatures of the snow pack, as well as other surfaces, are empirically investigated and then used in automated

separation algorithms. The use of automated techniques to accomplish image classification is especially beneficial in an operational remote sensing program.

Comparison of AVHRR and SSM/I images were made from images that view the same location at nearly the same time. Detailed surface classification of the AVHRR images was accomplished based on research conducted at the Naval Postgraduate School (NPS) by Allen *et al* (1990). This technique of AVHRR image classification has gained a high level of confidence and served as a "truth" or baseline for the SSM/I imagery. The SSM/I data was compared to the AVHRR classified image and the use of SSM/I imagery was examined as either a stand alone method for determination of extent of snow cover or as a supplement to AVHRR images.

II. THEORY

A. GENERAL

Energy is being released constantly by the sun in the form of electromagnetic radiation over a spectrum of wavelengths. The amount of energy released by a perfect blackbody is approximated by the Planck equation in the form of radiance:

$$B_\lambda(T) = \frac{2hc^2\lambda^{-5}}{\exp(hc/\lambda\ kt) - 1} \tag{2.1}$$

In this equation $B_\lambda(T)$ represents the radiance as a function of wavelength and temperature, h is the Planck constant, k is the Boltzman constant and c is the speed of light in m/s. Radiance in this expression is not dependent on viewing angle. True blackbodies exist in theory only and are seldom approached in nature. Emittance as a function of wavelength, ε_λ, describes the departure of an emitting surface from a perfect blackbody and is empirically obtained. Emittance is also a function of viewing angle.

Excluding Raman scattering or fluorescence, incident radiation on the surface of a body is either absorbed, reflected or transmitted. If the total incoming radiance is set at one then the sum of these three processes must be equal to one if energy is to be conserved. Kirchhoff's law states that a surface exposed to incident radiation will emit an amount of energy equal to the energy it absorbs if thermodynamic equilibrium is maintained. The earth's atmosphere is assumed to be in local thermodynamic equilibrium for this satellite application.

If the earth's atmosphere were a complete vacuum, a satellite viewing the earth from orbit would strictly measure the radiance from the surface. Depending on the physical

composition of the surface, this energy from the sun is reflected off of the surface or cause the amount of radiance measured at the satellite to differ from the value leaving the surface. The atmosphere can absorb radiation emitted from the surface or scatter the radiation away from the satellite sensor and lower the amount of energy received. It can also emit energy along the path from the surface to the sensor or scatter energy into the path from other sources to elevate the radiance measured above the amount actually leaving the surface. These processes occur simultaneously in the atmosphere and make the basic radiative transfer equation extremely complex:

$$L_T(\lambda,\theta,\varphi) = L_O(\lambda,\theta,\varphi)e^{-\delta(\lambda)/\mu} + \int_0^{\delta(\lambda)} J_*(\lambda,z,\theta,\varphi)/\sigma_e(\lambda,z)e^{-\delta(z,\lambda)/\mu}d\delta/\mu \qquad (2.2)$$

The term on the left hand side of the equation represents the total radiance arriving at the sensor as a function of wavelength along a slant path. The first term on the right hand side is the surface radiance multiplied by the direct transmittance through the entire atmosphere. The second term on the right hand side represents the radiance gained or lost along the slant path where J_* is the source function and σ_e is the extinction coefficient at each position multiplied by the direct transmittance to the top of the atmosphere. Simplifying assumptions made to this equation allow each pixel in a satellite image to be assigned a representative temperature or reflectance based on the radiance received at the satellite sensor.

Various surfaces, such as land or snow, absorb or reflect solar energy at differing levels and are measured as areal contrasts by the satellite. These differences, which are a function of wavelength, physical composition of the substance and sun-satellite viewing geometry, allow for image classification and form the basis of this thesis.

B. AVHRR IMAGERY

The theory of radiative transfer for AVHRR imagery is very well described by both Allen (1987) and Barron (1988). AVHRR satellites have sensors that receive upwelling radiance in specific wavelength bands that range from the visible to infrared spectrum. Channel 1, centered at 0.63 μm wavelength, is a visible channel. Channel 2 is centered at 0.87 μm and receives visible wavelength energy at longer wavelengths than channel 1. Channel 3, centered at 3.7 μm, senses a mixture thermal emission and solar reflection. Channel 4 is a pure thermal or infrared channel and is centered at a wavelength of 11.0 μm. Both channel 1 and 2 use reflectance as units of measure while channels 3 and 4 convert radiance into temperature.

Assuming no loss of signal from a viewed surface to the satellite sensor due to atmospheric absorption, optically thick clouds and no scattering the basic radiative transfer equation 2.2 reduces to:

$$L_T = \varepsilon B(t) + r(\theta_O, \theta, \varphi) I \cos\theta_O \qquad (2.3)$$

The term on the left hand side of the equation is the observed radiance at the satellite sensor. The first term on the right hand side of the equation is the surface term and represents the thermal emission emitted by a black body multiplied by the emissivity. The energy emitted by a perfect blackbody is given by the Planck function and the emissivity scales this output energy based on the physical characteristics of the surface. The second term on the right hand side ($I\cos\theta_O$) is a solar reflectance term and is a function of the normalized incident solar radiation multiplied by the reflectance from the viewed surface ($r(\theta_O, \theta, \varphi)$). This simplified radiative transfer equation will be the basis of all AVHRR analysis presented in this study.

1. Channel 1

Since Channel 1 is strictly a visible light channel, the thermal emission term of the radiative transfer equation 2.3 is zero. Therefore radiance measured in Channel 1 is generated entirely by the reflectance of the viewed surface. The amount of radiance received is dependent on the physical properties of surface being observed. It is also highly dependent on the solar and satellite zenith angles as well as the azimuth that separates these two angles. Reflection is generally measured as a non-dimensional quantity known as albedo. Albedo is the ratio of radiant exitance to irradiance and is a value that varies between zero and one. The CD-ROM data used for the AVHRR imagery in this thesis used a scaled albedo that varied between 0 and 64 percent. That is, the minimum albedo of zero was represented by a gray shade of zero while the maximum albedo represented was 64 percent. These maximum and minimum albedos correspond to gray shade levels of zero and 255 respectively. The NOHRSC User's Guide (1990) provides the necessary conversion factors to change the gray shade image into binary reflectance data.

Figure 2.1 shows a channel 1 image from NOAA 11 that viewed the Great Lakes region of the United States on 20 February 1990. Table 2.1 lists various albedos based on differing surfaces as taken from figure 2.1.

Darker colored surfaces (bare soil, lakes) have low albedos while lighter colored surfaces (snow, clouds) have higher albedos. Because the reflectance is so dependent on viewing geometry, it is an unreliable parameter when used as a single separation threshold for surface classification except for very strong contrasts such as snow and bare ground. It is very useful when combined with other values such as surface temperature.

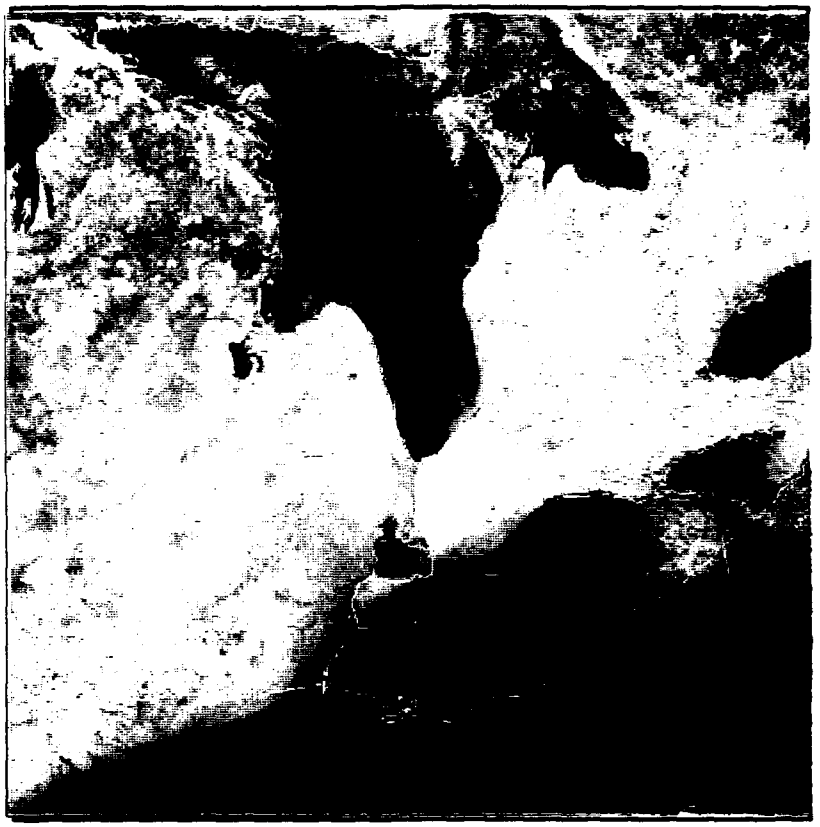

Figure 2.1- 20 February 1990 channel 1 image over the Great Lakes region.

TABLE 2.1 - CHANNEL 1 SCALED ALBEDO EXTRACTED FROM FIGURE 2.1.

SURFACE	MAX.	MIN.
LAND	8.0	3.0
LAKE	5.0	0.0
SNOW	33.0	15.0
SNOW IN TREES	28.0	7.0
CU CLOUD	37.0	14.0
THIN CIRRUS	25.0	9.5

Table 2.1 indicates that very large channel 1 reflectance differences are found between land without snow and land covered with snow. Similarly, the Great Lakes show extremely low albedo due to the low sun elevation at the time of the satellite pass

and the strong absorptive properties of water and are easily distinguished from snow covered land. Clouds and snow covered land have nearly identical albedos and are very difficult to distinguish when viewed in channel 1.

2. Channel 2

Channel 2 is a near-infared channel and is wavelength centered at $0.87\,\mu\,m$. The channel 2 data is also calibrated in terms of scaled albedo and was converted to gray shade from CD-ROM to the VAX computer using the conversion factors provided in the NOHRSC CD-ROM User's Guide. Again, all the radiance measured by channel 2 comes from the reflectance term of equation 2.3.

Figure 2.2 shows the same subscene as figure 2.1 viewed in channel 2. The channel 1 and channel 2 images are nearly identical but there are some subtle differences. The channel 2 image is slightly darker than the channel 1 subscene except over areas of land covered with vegetation. This is because the vegation found on land surfaces is a stronger absorber in channel 1 than in channel 2. Table 2.2 lists various surface albedos taken from figure 2.2. Use of the small differences found in the albedos between channels 1 and 2 will be applied in the separation algorithm to distinguish land uncovered with snow and lakes.

Figure 2.2 - 20 February 1990 channel 2 image over the Great Lakes region.

TABLE 2.2 - CHANNEL 2 ALBEDO EXTRACTED FROM FIGURE 2.2.

SURFACE	MAX.	MIN.
LAND	13.0	3.5
LAKE	5.0	0.0
SNOW	33.0	9.0
SNOW IN TREES	18.0	1.0
CU CLOUD	35.0	11.0
THIN CIRRUS	24.0	5.0

3. Channel 3

Channel 3 is perhaps the most important AVHRR channel used when conducting multi-spectral analysis for image classification because it allows for the distinction of liquid clouds over snow covered land. Calibrated in radiance, the brightness temperature

derived from this channel will generally have contributions from both solar reflectance and thermal emission during daytime satellite passes. The amount of radiance received from solar reflection as compared with thermal emission is a function of the properties of the emitting or reflecting surface as well as the satellite-sun viewing geometry. Allen (1987) found that the solar reflection term of equation 2.3 is the dominant daytime term for most liquid clouds while ice clouds, snow and land had nearly equal contributions from solar reflectance and thermal emittance.

Figure 2.3 presents a channel 3 view of the same subscene as figure 2.1 with brightness temperatures converted to gray shade. Liquid clouds are clearly the brightest features of this image due to the magnitude of the solar reflectance term in equation 2.3. In contrast, snow covered land has faded from view and shows an almost unnoticeable contrast with snow free land. Compared with the images of channels 1 and 2, the snow has disappeared. Table 2.3 presents typical surface values extracted from figure 2.3.

TABLE 2.3 - CHANNEL 3 TEMPERATURES IN DEGREES KELVIN EXTRACTED FROM FIGURE 2.3.

SURFACE	MAX.	MIN.
LAND	285.0	271.0
LAKE	275.0	271.5
SNOW	275.0	271.0
SNOW IN TREES	275.0	271.0
CU CLOUD	307.0	280.0
THIN CIRRUS	268.0	252.0

The brightness temperatures displayed show the large temperature difference between liquid clouds and any other surface. This strong temperature difference is dependent on sun-satellite viewing angle. In general liquid clouds will remain the brightest surface on the image regardless of sun angle except for cases of sunglint over water or melting snow.

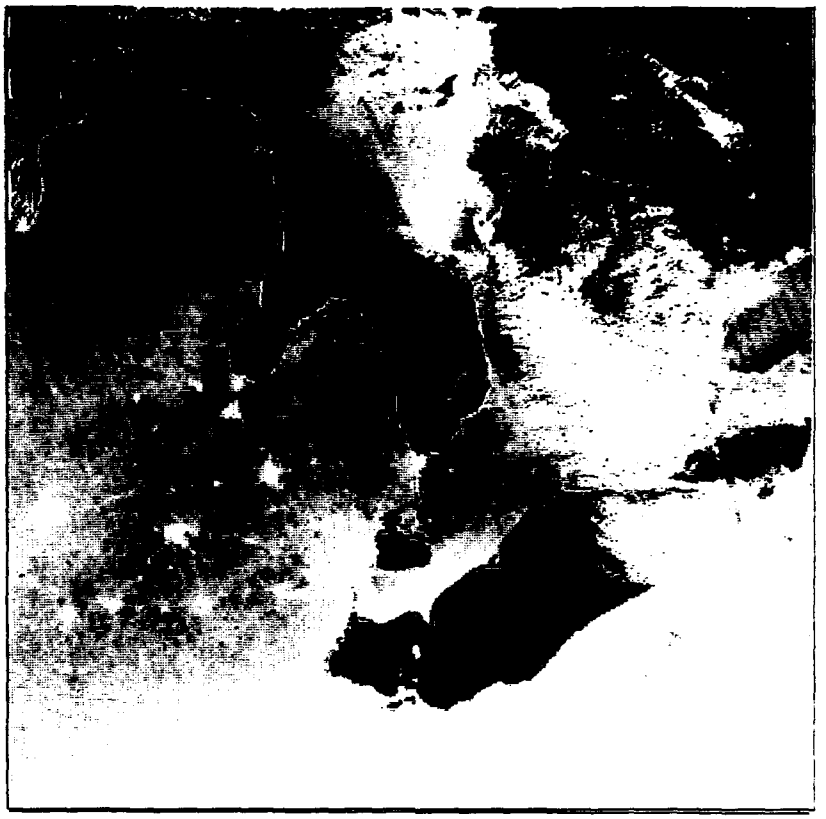

Figure 2.3 - 20 February 1990 channel 3 image over the Great Lakes region.

4. Channel 4

The brightness temperatures retrieved by channel 4 are derived from wavelengths beyond direct solar contribution which allows the solar reflectance term of equation 2.3 to be dropped. This means that channel 4 is strictly a measure of the thermal emittance. Figure 2.4 shows the same subscene imaged in figure 2.1 as viewed in channel 4. Channel 4 is sensitive to water vapor in the atmosphere and this effect is amplified in regions of warm, humid air since warm air is capable of holding more moisture than cold air. Allen (1987) suggests that the attenuation of infrared signal due to water vapor can be considered negligible due to the cold, dry conditions normally found in winter

environments. This type of atmospheric condition prevails in polar-type highs that often follow cold front passage in the Great Lakes region of the United States.

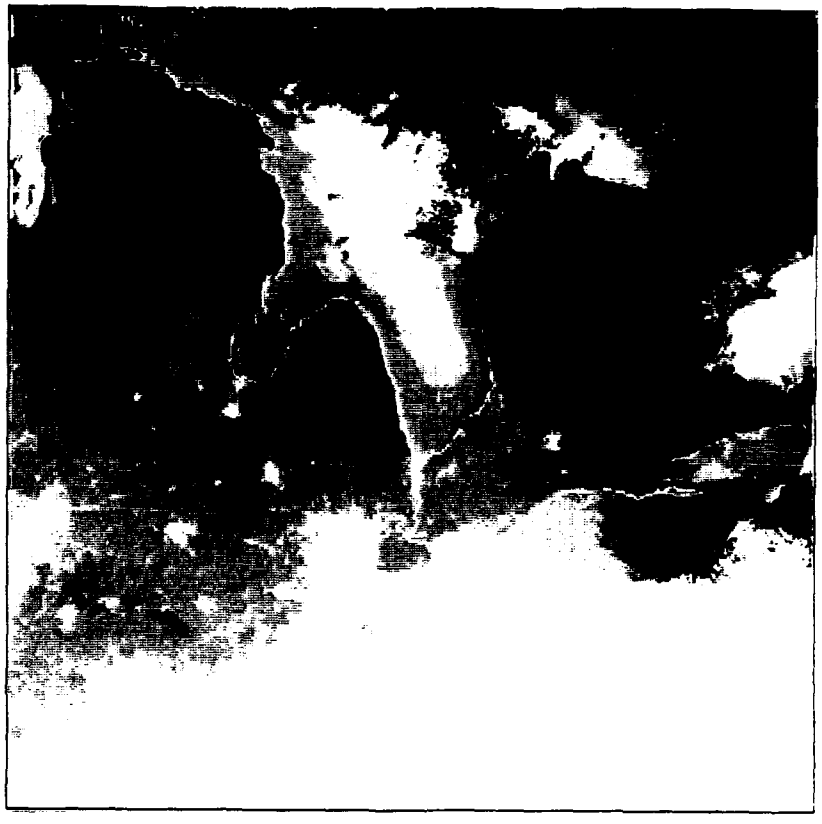

Figure 2.4 - 20 February 1990 channel 4 image over the Great Lakes region.

Since channel 4 measures the thermally emitted temperature of a surface it is used to detect very cold, high clouds by using a single temperature threshold. It is reasonable to assume that surfaces that are extremely cold are not located on or very near the ground. Table 2.4 shows the brightness temperatures extracted for various locations of figure 2.4.

TABLE 2.4 - CHANNEL 4 TEMPERATURE IN DEGREES KELVIN EXTRACTED FROM FIGURE 2.4

SURFACE	MAX.	MIN.
LAND	274.0	264.0
LAKE	274.0	270.0
SNOW	271.0	268.0
SNOW IN TREES	270.0	268.0
CU CLOUD	270.0	258.0
THIN CIRRUS	262.0	235.0

5. AVHRR Channel Differencing

The representative albedos and temperatures presentented in this section show that differences exist between channels that may be exploited to identify various surfaces. Specifically, the channel 2 minus the channel 1 reflectance difference and the channel 3 minus the channel 4 brightness temperature difference can be used to identify land and liquid cloud, respectively.

Table 2.5 gives the result of the channel 2 minus the channel 1 difference of the albedos given in Tables 2.1 and 2.2. Land has a distinctly positive channel 2 minus channel 1 albedo difference due to the stronger absorption of visible light in channel 1 by vegetation. All other surfaces listed have no difference or a negative albedo difference. The uniquely positive albedo difference for land makes it possible to separate land pixels from lake pixels, which have nearly the same reflectance and brightness temperature in channel 1 and channel 4, respectively.

The channel 3 minus the channel 4 brightness temperature difference allows for a first order estimate of the solar reflectance by simply subtracting the channel 4 from the channel 3 brightness temperature. This procedure basically eliminates the thermal emittance term of equation 2.3 leaving just the solar reflectance contribution of channel 3.

TABLE 2.5 - REPRESENTATIVE CHANNEL 2 MINUS CHANNEL 1 ALBEDO DIFFERENCES.

SURFACE	MAX.	MIN.
LAND	5.0	0.5
LAKE	0.0	-2.0
SNOW	0.0	-6.0
SNOW IN TREES	-6.0	-10.0
CU CLOUD	-2.0	-4.0
THIN CIRRUS	-1.0	-4.5

Since the most dominant feature of the channel 3 image is the solar reflectance from liquid clouds, this subtraction routine provides an excellent method to isolate these clouds that may overlie snow and have of similar channel 1 and 2 reflectance. Table 2.6 gives a representive result of the channel 3 minus channel 4 brightness temperature difference for various surfaces.

TABLE 2.6 - REPRESENTATIVE CHANNEL 3 MINUS CHANNEL 4 BRIGHTNESS TEMPERATURE DIFFERENCES.

SURFACE	MAX.	MIN.
LAND	11.0	7.0
LAKE	1.5	1.0
SNOW	4.0	3.0
SNOW IN TREES	8.0	1.0
CU CLOUD	37.0	22.0
THIN CIRRUS	17.0	6.0

C. SSM/I IMAGERY

The interest in viewing the snow pack with microwave imagery is motivated by the fact that the atmosphere is nearly transparent to high frequency radiation. The all weather capability of microwave remote sensing of the areal extent of snow cover is particularly attractive in the winter months, when cloud cover can obscure the ground for days making AVHRR imagery of the surface impossible.

There are two major problems that prevent microwave imagery from being more useful as a remote sensing tool. The first is that at centimeter wavelengths the emission is low at the tail of the Planck function. While nearly all surfaces emit microwave radiation, they do so in small amounts compared to the infrared part of the spectrum. The second is that the antenna used to capture this relatively weak signal must be restricted in dimension due to the physical size restraints of the spacecraft. Depending on the selected frequency the result is an image that is roughly ten to 40 times poorer in resolution than a similar AVHRR image.

The passive microwave radiative transfer equation can be considered as a special case of equation 2.2 depending on whether the selected frequency of interest resides in a window or non-window region. A window region is considered to exist at frequencies below 50 GHz, while a non-window region is approximated at frequencies above 50 GHz. Since the 37 and 85 GHz frequencies have been selected for use in this study, both cases will be considered.

The Planck function, equation 2.1, is modified in the microwave portion of the spectrum by the application of the Rayleigh-Jean approximation and can be expressed as follows:

$$B(\nu,T)=\frac{2k\nu^2}{c^2}T \tag{2.4}$$

In this equation the radiance is a function of frequency and body temperature. Recalling that the Planck function describes a perfect black body, a more appropriate expression of the radiance in the presence of no atmosphere would be:

$$L=E_sB(\nu,T)=\frac{2k\nu^2}{c^2}E_sT_s \tag{2.5}$$

Multiplying both sides of equation 2.5 by $c^2/2k\nu^2$ the brightness temperature, T_B can be defined as:

$$T_B = L\frac{c^2}{2k\nu^2} \Rightarrow T_B = E_s T_S \tag{2.6}$$

This suggests that the brightness temperature, expressed as the surface temperature multiplied by the surface emissivity, can be substituted into equation 2.1.

At a given frequency the emissivity of a surface, E_s , is dependent on the physical composition of the surface and its temperature. Since Fresnel reflectance is a function of polarization, there is a need to split the polarization into a horizontal and vertical component. The horizontal component can be expressed as one minus the horizontal reflectance, or:

$$E_H(\nu) = 1 - \rho_H(\nu) \tag{2.7}$$

Similarly the vertical component is:

$$E_V(\nu) = 1 - \rho_V(\nu) \tag{2.8}$$

This implies that the brightness temperature is also split into horizontal and vertical components, or that $T_B \Rightarrow T_{BH}, T_{BV}$. Because the horizontal and vertical emissivities are dependent on zenith angle it is understood that the respective brightness temperatures are also angle dependent.

Microwave radiation may originate from the surface and be transmitted directly through the atmosphere to the sensor. It may also be emitted by the atmosphere in a downward direction and then reflected off the surface, or it may be emitted directly from the top of the atmosphere to the sensor. For frequencies less than 50 GHz in a homogeneous atmosphere the radiative transfer equation can be rewritten as:

$$T_B(\nu,\theta,\varphi)=E_s(\nu,\theta,\varphi)T_s e^{\frac{-\delta(\nu)}{\mu}}+[1-E_s(\nu,\theta,\varphi)]T_{air}[1-e^{\frac{-\delta(\nu)}{\mu}}]e^{\frac{-\delta(\nu)}{\mu}}+T_{air}[1-e^{\frac{-\delta(\nu)}{\mu}}] \tag{2.9}$$

The term on the left hand side of the equation is the brightness temperature as a function of frequency, angle off nadir, and azimuth angle. The first term on the right hand side is the radiation emitted from the surface and transmitted directly through the atmosphere. The second term on the right hand side of the equation is downward emitted radiation from the atmosphere that is reflected by the surface and then transmitted through the atmosphere to the satellite. The third term represents radiation emitted by the top of the atmosphere.

Since frequencies less than 50 GHz are considered to be located in the window region, atmospheric scattering can be assumed to be zero. Absorption, α, is then equal to one minus the transmittance, or:

$$\alpha=1-\tau=1-e^{\frac{-\delta(\nu)}{\mu}} \tag{2.10}$$

Because this regime is considered to be an atmospheric window, transmittance is assumed to approach one and therefore atmospheric absorption, α, can assumed to be small. This implies that terms two and three of equation 2.9 are very small so that the atmospheric contribution to the total radiance received at the sensor can be considered negligible.

At frequencies greater than 50 GHz the atmosphere should not be considered homogenous and may have a measurable contribution to the signal received at the satellite sensor. In that case terms two and three of equation 2.9 should be integrated downward and upward with appropriate weighting functions to account for atmospheric contributions to the signal. While scattering of microwave radiation by atmospheric gases is considered to be small in this frequency range, absorption by liquid water and water vapor may affect transmittance.

It is evident that the atmosphere has little effect on microwave frequencies below 50 GHz but may significantly contribute to frequencies above 50 GHz. This is unfortunate since the frequency of greatest horizontal resolution, 85 GHz, falls into the non-window range.

Mie scattering can significantly attenuate both frequency regimes. Table 2.7 gives the approximate size of particles necessary to produce Mie scatter for the four frequencies utilized by the DMSP SSM/I satellite. A typical cloud drop radius is of order magnitude 0.001 cm while that of a normal raindrop is of order magnitude 0.1 cm. Clearly in the Mie scattering regime, cloud drops have very little effect on passive microwave radiation but precipitation can cause significant scattering.

TABLE 2.7 - APPROXIMATE PARTICLE SIZE NECESSARY TO PRODUCE MIE SCATTER FOR THE FOUR SSM/I FREQUENCIES.

FREQUENCY (GHz)	WAVELENGTH (CM)	RADIUS (CM)
85	0.35	0.11
37	0.81	0.26
22	1.36	0.43
19	1.58	0.50

Microwave energy released from the surface of the earth is affected by an overlying snow pack. The snow pack itself is a weak emitter of microwave radiation. Kong *et al* (1979) determined that snow behaves as a Mie volume scatterer. They noted that the brightness temperature received from a snow covered target was a function of the surface underlying the snow, the snow depth, frequency, polarization and angle of incidence. They also observed that brightness temperature decreased as snow depth increased when snow covered a subsurface of soil. Due to the estimated size of the individual snow crystals this effect is particularly pronounced for shorter wavelengths. Longer

wavelengths are less affected by the presence of snow, and are influenced more by the composition of the underlying surface.

Srivastav and Singh (1991) modeled the changes of the brightness temperature of wet and dry snow fields by incorporating a changing complex dielectric parameter. They showed that at frequencies above 15 GHz a contrast was found between wet and dry snow. At these frequencies the contrast in brightness temperature between wet snow and dry land was minimal but the brightness temperature of dry snow became increasingly depressed with increased frequency. Also studied was the difference in brightness temperatures between two polarizations of the same frequency. At 37 GHz, it was noted that the temperature difference decreased slowly to near zero for bare ground. The polarization differences also decreased for wet and dry snow at 37 GHz but the differences remained strongly positive, especially for dry snow.

Kunzi *et al* (1982) conducted early examinations of snow with Scanning Multi-channel Microwave Radiometer (SSMR) observational data. They noted that liquid water, with its high dielectric loss, significantly attenuates the signal emitted from the underlying soil suggesting that wet snow would show reduced brightness temperatures. The primary loss of signal in dry snow was again noted to be caused by volume scattering. One and two dimension measurement space analysis was conducted on the data sets and image classification was accomplished. It was noted that the variance for the horizontal brightness temperatures was larger than that of the vertical brightness temperatures. Additionally, it was discovered that it was impossible to distinguish areas with very wet soil from areas covered with snow using a one dimensional analysis and that in all channels melting snow may have the same brightness temperature as snow free land. Finally, it was established that multi-spectral analysis was the best technique for

surface classification and that separation of land and snow was possible if the snow depth was approximately five cm or deeper.

McFarland *et al* (1987) conducted a comprehensive study of snow in the Great Plains of the United States using 1978-1979 winter SSMR data. They observed significant depression of the 37 GHz brightness temperatures when the ground was covered by dry snow at an accumulation depth of approximately two cm. A depression of brightness temperature was noted in both long and shorter wavelengths for snow accumulation up to 20 cm. Volume scattering from the snow crystals caused the lowering of brightness temperature in the shorter wavelengths while lowered temperatures in the longer wavelengths were thought to be caused by surface cooling below the snow pack and increased reflectivity of the low background temperature of space. Significant increase of the 37 GHz brightness temperature polarization difference was discovered starting at snow depths of two cm and continued in a near linear fashion to snow depths of 15 cm. Maximum scattering was reached at 15 cm, and no further increase in scattering was noted in snow of greater depth than 15 cm. Variations of the brightness temperature polarization differences were also observed during the snow ripening and melting phases, as well as during the diurnal cycle.

This study will concentrate on the determination of the areal extent of snow cover using the 37 and 85 GHz channels. Using the AVHRR imagery as a guide, surfaces in the SSM/I images will be identified multi-spectrally and thresholds will be determined and then applied to an automated classification routine. The steps involved in accomplishing the SSM/I image classification are essentially the same as for separation of the AVHRR data. The use of only the 37 and 85 GHz data is primarily driven by the desire to keep the resolution of the microwave data as high as possible. Unfortunately, the 85 GHz channel from the DMSP spacecraft for the period under study contains

corrupted 85 GHz vertical polarization data due to a partial sensor failure. Therefore the multi-spectral analysis will employ the 37 GHz vertical and horizontal and the 85 GHz horizontal polarized brightness temperatures.

1. 37 GHz Horizontal Channel

The 37 GHz horizontal channel is composed of 0.81 cm wavelength radiation. The spatial resolution of this data is approximately 38 x 40 km at an earth incidence of 53 degrees (Spenser *et al* 1989). Figure 2.5 shows the same approximate subscene as AVHRR figure 2.1 approximately six hours earlier than figure 2.1.

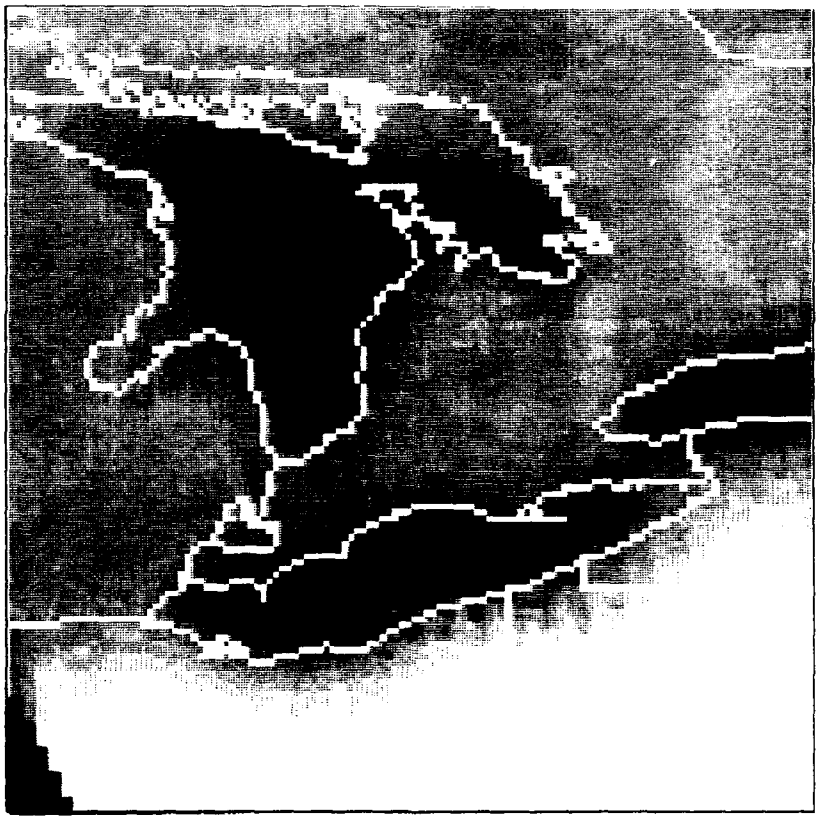

Figure 2.5 - 20 February 1990 37 GHz horizontally polarized image over the Great Lakes region.

Lighter shaded surfaces represent warmer brightness temperatures. Extremely cold surfaces may be distinguished as part of the Great Lakes due to the low emissivity of the water. Land and snow covered land show possible variation due to the volume scattering effect of the snow that causes the snow covered land to be darker due to depressed brightness temperatures. Table 2.8 presents representative brightness temperatures of surfaces extracted from this image by using positions taken from the associated AVHRR image. The resolution of this image makes it hard to distinguish different environmental features and indicates the difficulty associated with separation based on single dimension spectral analysis using 37 GHz channels.

TABLE 2.8 - 37 GHz HORIZONTALLY POLARIZED BRIGHTNESS TEMPERATURES EXTRACTED FROM FIGURE 2.5.

SURFACE	MAX.	MIN.
LAND	259.0	249.0
LAKE	161.0	130.0
SNOW	221.0	200.0

2. 37 GHz Vertical Channel

The 37 GHz vertical polarization brightness temperature is shown as figure 2.5 for the same spatial area as figure 2.1. Resolutions are the same as in the 37 GHz horizontal case. The vertically polarized brightness temperatures are generally higher than the horizontally polarized brightness temperatures and it is therefore convention to subtract the horizontal from the vertical brightness temperature to obtain the brightness temperature polarization difference. Table 2.9 presents brightness temperatures of representative surfaces extracted from the figure 2.6. Again the resolution of the vertical 37 GHz image suggests that the most useful application of this data is either as a difference product or in combination with a different frequency.

Figure 2.6 - 20 February 1990 37 GHz vertically polarized image over the Great Lakes region.

TABLE 2.9 - 37 GHz VERTICALLY POLARIZED BRIGHTNESS TEMPERATURES EXTRACTED FROM FIGURE 2.6.

SURFACE	MAX.	MIN.
LAND	264.0	256.0
LAKE	212.0	201.0
SNOW	241.0	220.0

3. 85 GHz Horizontal Channel

The 85 GHz horizontal channel represents a major improvement in resolution over the 37 GHz frequency. Figure 2.7 shows the 85 GHz horizontal image which spatially and temporally approximates figure 2.1. According to Spencer *et al* (1989), the spatial

resolution obtained from the 85 GHz channels is approximately 16 x 14 km at an earth incidence of 53 degrees. The improvement in resolution makes the 85 GHz channel much easier to interpret geographically. Once again the Great Lakes show the lowest brightness temperatures and form the darkest parts of the image. Also noticeable, especially when positioned over water, is precipitation that is warmer than the water that it overlies. The presence of precipitation over land is much less discernible, making surface separation less distinctive.

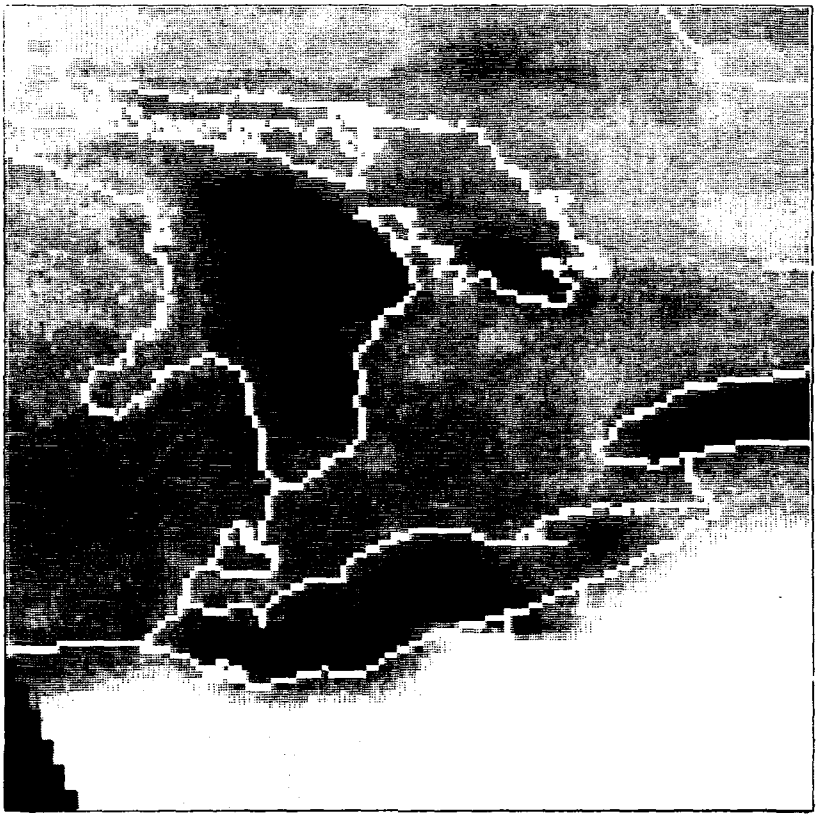

Figure 2.7 - 20 February 1990 85 GHz horizontally polarized image over the Great Lakes region.

The snow line appears to be almost visible as the warmer uncovered land transitions into colder snow covered land. This effect of the snow as a volume scatterer

at 85 GHz shows up very strongly along the latitude of the lower Great Lakes. The possibility of assigning single brightness temperature thresholds to separate the snow, snow free land and water of the Great Lakes is attractive. Table 2.10 presents the brightness temperatures extracted from figure 2.7.

TABLE 2.10 - 85 GHz HORIZONTALLY POLARIZED BRIGHTNESS TEMPERATURE EXTRACTED FROM FIGURE 2.7.

SURFACE	MAX.	MIN.
LAND	264.0	247.0
LAKE	193.0	170.0
SNOW	221.0	185.0

4. SSM/I Channel Differencing

The SSM/I channels, like the AVHRR data, can also be differenced to gain additional information about the characteristics of emitting surfaces. As reported by McFarland *et al* (1987), the 37 GHz vertically polarized channel minus the 37 GHz horizontally polarized channel brightness temperature difference becomes strongly positive in the presence of snow. This is because the volume scattering of the snow pack attenuates the microwave signal of the underlying soil more in the 37 GHz horizontal channel. Table 2.11 shows representative channel 37 GHz vertically polarized minus 37 GHz horizontally polarized brightness temperatures.

TABLE 2.11 - REPRESENTATIVE 37 GHz POLARIZATION BRIGHTNESS TEMPERATURE DIFFERENCES.

SURFACE	MAX.	MIN.
LAND	7.0	5.0
LAKE	71.0	51.0
SNOW	20.0	0.0

Additionally, the 85 GHz horizontally polarized channel minus the 37 horizontally polarized brightness temperature difference was investigated. The observation made by Kunzi *et al* (1982) that shorter microwave wavelengths are more scattered by the snow pack than longer wavelengths is applied. Ferraro *et al* (1986) demonstrated that dry snow caused a negative 37 minus 18 Ghz vertically polarized brightness temperature difference. This research attempts to extend these theories to a set of higher resolution microwave channels, i.e., the 85 minus the 37 GHz horizontally polarized brightness temperature difference. Table 2.12 gives the representative brightness temperature differences of the 85 minus the 37 horizontally polarized channels for various surfaces.

TABLE 2.12 - REPRESENTATIVE 85 MINUS 37 GHz HORIZONTALLY POLARIZED BRIGHTNESS TEMPERATURES.

SURFACE	MAX.	MIN.
LAND	5.0	-2.0
LAKE	40.0	32.0
SNOW	0.0	-15.0

III. PROCEDURE

A. OVERVIEW

General theory presented in chapter two demonstrates that surfaces such as cloud, land or snow emit or reflect radiation as a function of their physical composition. In many instances the radiative signature of these surfaces in the various AVHRR and SSM/I channels are not unique, making it appear that surface separation from remote sensing radiation contrasts would not be possible. Closer inspection reveals that given enough parameters of measurement, major emitting surfaces display different characteristics that can be exploited in image classification. The use of high speed computers to examine an image pixel by pixel in several channels simultaneously brings almost unnoticed differences to light and allows for major surface distinction.

Images were individually examined and the characteristics of each major surface was measured in AVHRR channels 1, 2, 3 and 4 as well as in the 35 GHz and 85 GHz channels of SSM/I. Differences observed in temperature and reflectance were then used to set thresholds in a logical sequence of decisions which resulted in classification. Throughout this thesis the AVHRR images served as a baseline for SSM/I comparison.

Both AVHRR and SSM/I separation algorithms were developed using data from the Great Lakes region of the United States. They were then tested in the western United States using six additional subscenes. Modifications were then made to the algorithms and then all cases were run again using a single AVHRR and a single SSM/I algorithm.

B. PROCESSING AVHRR DATA

All AVHRR images studied in this thesis were extracted from the NOAA NOHRSC 1990 Airborne and Snow Data CD-ROM which features 15 North American satellite regions used to determine the areal extent of snow cover during the snow season. Figure 3.1 shows the location of the AVHRR windows established by the NOHRSC. The NOHRSC CD-ROM is prepared each year as an historical document and tool for snow measurement research. This product includes calibrated, georegistered, eight bit satellite image data of the areal extent of snow coverage on dates where snow cover was observable. Additionally, low level aircraft snow pack measurements are included on the CD-ROM.

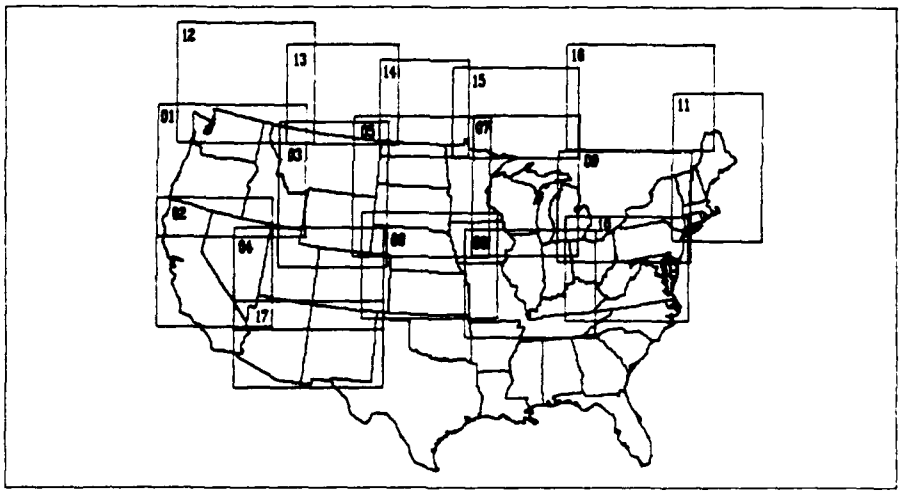

Figure 3.1 - NOHRSC snow mapping windows. From Carroll (1990).

The inherent advantage of the CD-ROM is that any appropriately equipped personal computer (PC) can access many satellite images in a short period of time. Compared to a nine track or DAT tape format, the ability to move from image to image on the CD-ROM is very useful. Every image on the 1990 NOHRSC CD-ROM was viewed and a

particular window and date was selected based on snow cover, distinct snow line and cloud conditions. These selected images, which were comprised of channel 1, 2, 3 and 4 for each date, were then transferred from a PC to the NPS IDEA LAB Digital VAX computer system using the Net File Transfer (NFT) interface. The window images, approximately 800 lines by 1000 pixels in size, were cut into 512 by 512 pixel subscenes and navigated using program CD_PREPROCESS. The 512 by 512 images were then converted from gray shade to reflectance or temperature data using the conversion factors provided in the NOHRSC CD-ROM User's Guide (1990) and implemented in program CD_TO_REAL.

Once each pixel on the image was assigned an appropriate reflectance or temperature, sets of images were graphed as scatterplots in various channel combinations using program GET_DATA and NCAR graphics. Appendix A and B contains one set each of representative AVHRR and SSM/I scatterplots. These plots gave an overall view of the data in an easily assimilated format. The next step was to examine various subscenes of a particular image which were believed to be composed of a particular physical substance, such as land, snow, or cumulus clouds using program SURVEY and GET_ASCII. These programs plotted the distinct surfaces viewed as bi-spectral scatter plots and were then compared to the overall scatter plot of the entire image.

Threshold temperatures and reflectance were assigned to surfaces identified in the image from the evaluation of subscene scatter plots. Program CLASSIFU then used these thresholds in a logical block-if statement that tested and classified every pixel in the image. Each classified pixel in the new composite image was assigned a known gray shade value which allowed a color mask to be created using VAX resident image enhancement programs.

1. AVHRR Separation Agorithm

The AVHRR separation algorithm was developed from six subscenes that were extracted from AVHRR passes over the Great Lakes region of the United States on 31 January, 11 February and 20 February, 1990. Approximately 35 scatter plots were generated for each case using the bi-spectral combinations listed in table 3.2. Temperature and reflectance thresholds were identified for individual surfaces such as land or snow. The temperature and reflectance of each surface was also examined as the result of channel differencing. Specifically the channel 3 minus channel 4 and the channel 2 minus channel 1 difference was calculated for each surface. The goal of this analysis was to find a set or combination of measurements that was unique for each surface so that separation could be accomplished.

A logical block-if statement forms the basis of the separation algorithm that builds a composite image resulting from combinations of selected thresholds. The block-if statement moves through every pixel location in a 512 by 512 image and asks a series of questions about the surface observed at that particular pixel. At this point the algorithm is truly multi-spectral. Four 512 by 512 data arrays are read into the separation program and form the information base necessary at each pixel location for surface separation to be made. These arrays are the channel 1 reflectance, the channel 4 temperature, the channel 3-4 temperature difference and the channel 2-1 reflectance difference. Figure 3.3 shows a schematic of the data bases formed at each pixel location.

In the logical block-if statement each pixel is only allowed to pass through the decision tree once. If the surface at a given pixel location satisfies any of the statements of the block-if it is assigned a known gray shade and removed at that point from further

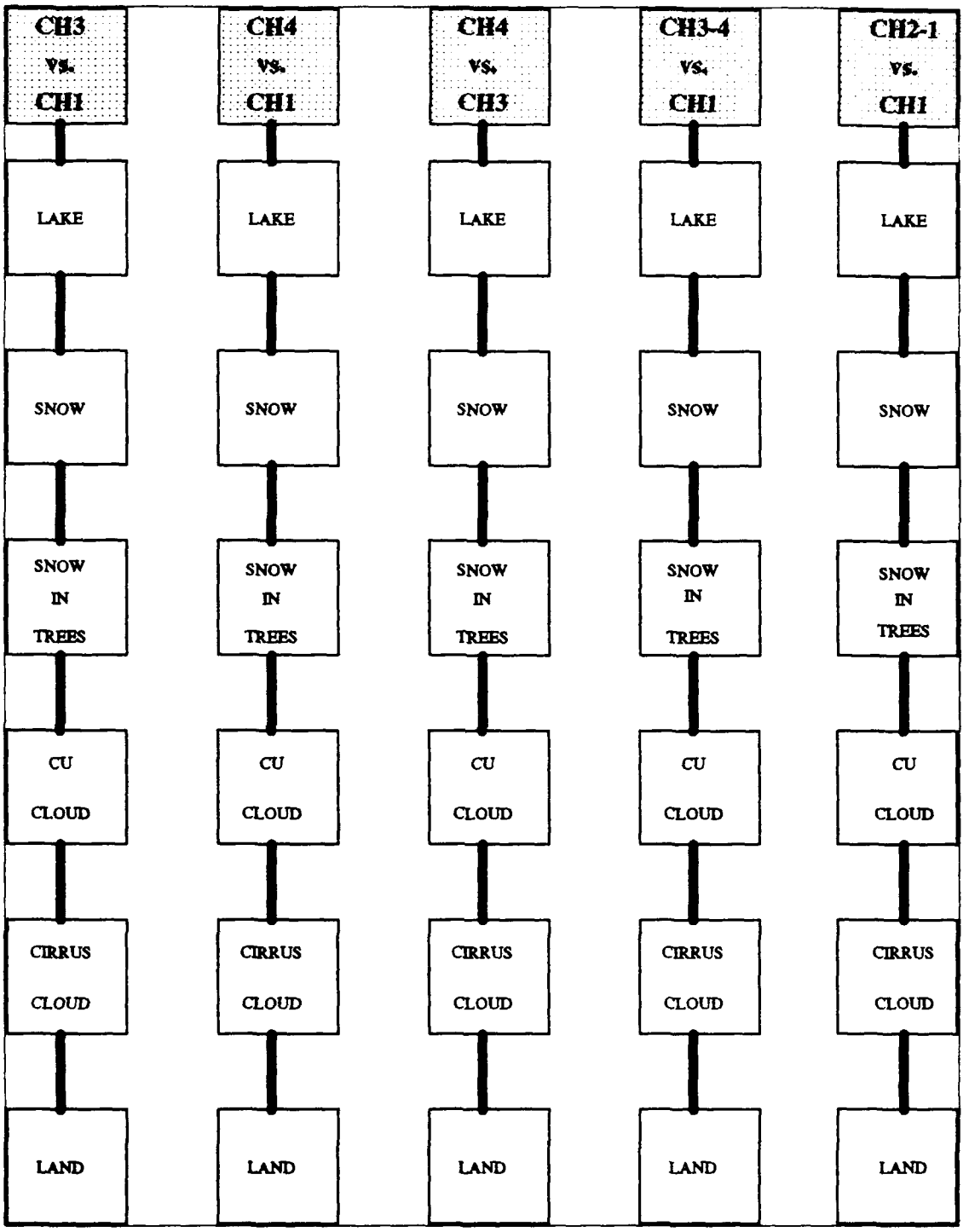

Figure 3.2 - AVHRR family of scatterplots.

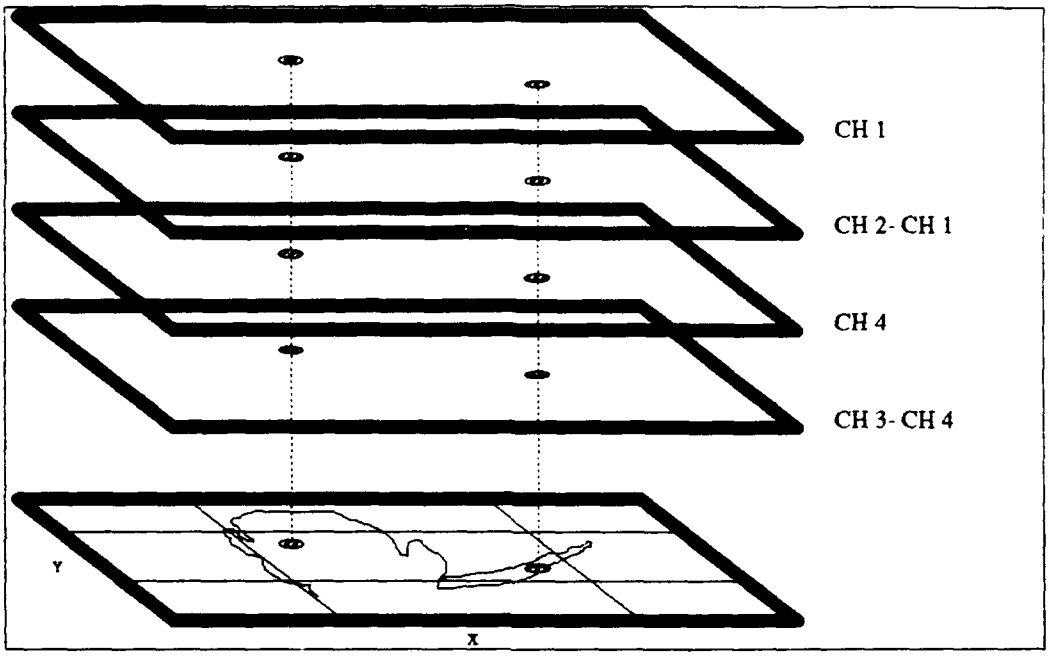

Figure 3.3 - Stacking of the 512x512 data arrays at each pixel location in program CLASSIFU.

consideration. If the pixel does not satisfy a given statement in the block-if, it continues to move down the decision tree until it becomes classified or it moves completely through the block-if without being selected. Pixels that pass completely through the block-if statements are assigned a gray shade that will also allow identification as an unclassified mixed pixel. The end product of the classification routine is a new composite image formed of distinct gray shades. Since the exact gray shading of a surface is now known, it is very easy to color the image by surface using program PSD.

Figure 3.4 is a schematic of the block-if section of the separation algorithm with each statement being represented by an enclosed rectangle. Each pixel enters at the top and filters down through the statements where it is eventually classified as a surface or labeled as a unclassified mixed pixel. A total of eight steps or statements are used in the algorithm.

The first step checks the channel 4 temperature at the given pixel location. Since very cold channel 4 temperatures would not normally be found on the ground a single temperature threshold is set to remove all high clouds from further steps in the logical block-if. This step is one of the few single value thresholds in the separation routine.

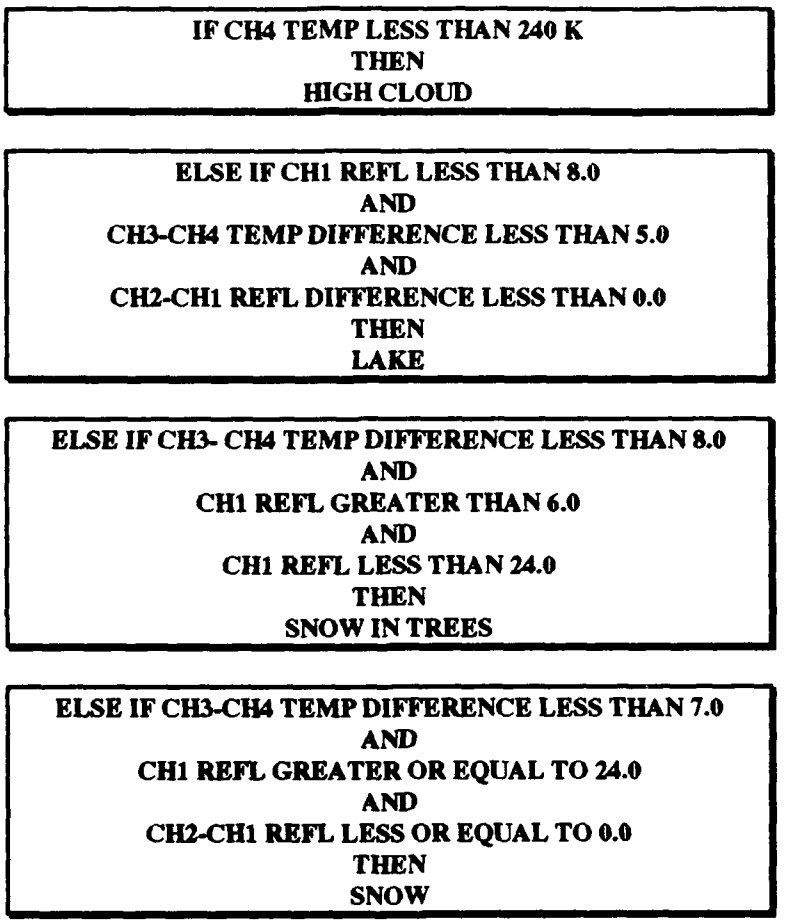

Figure 3.4 A - Program CLASSIFU logical decision path.

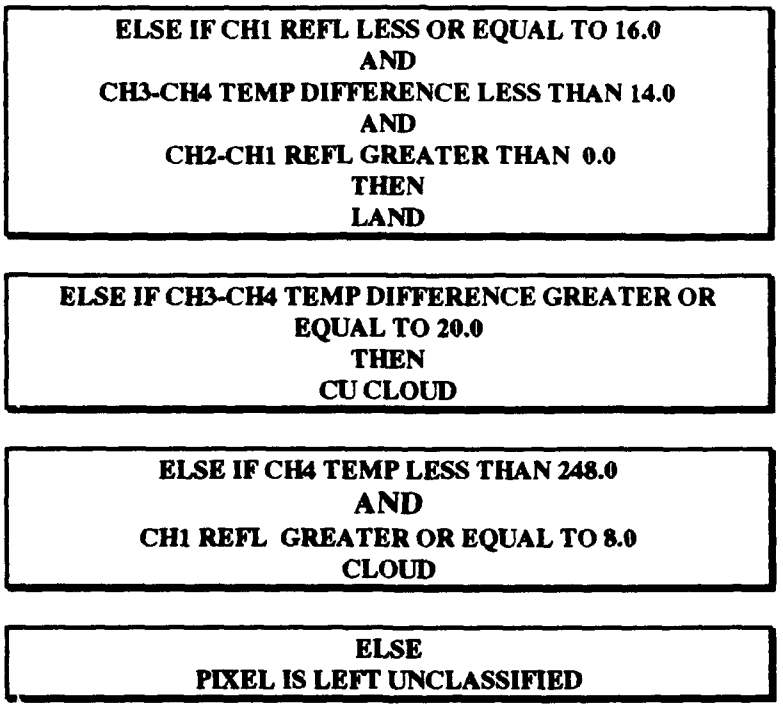

Figure 3.4 B - Program CLASSIFU decision path (continued).

The second step is a test to check if the pixel is a lake or open water pixel. This type of pixel was abundant in the Great Lakes region and needed to be identified. The lake regions could have been removed by simply masking them out using a mapping routine but this would not have made the algorithm sensitive to water that may exist elsewhere on the image. In this step several questions are asked and all must be satisfied in order for the pixel to be classified as a lake pixel.

The lakes were imaged without sun glint and consequently had the lowest channel 1 and 2 albedos of any viewed surface. Additionally, little variation was found between the channel 3 and channel 4 temperatures because solar reflectance term of equation 2.3 could be considered to be negligible. Finally the channel 2-1 reflectance difference had to be negative for classification as a lake pixel. This was a valuable tool in separating lake pixels from land pixels. The lake and land pixels are nearly identical when the arguments

of reflectance and channel 3-4 temperature differences are used but it was found that only land had a positive 2-1 reflectance difference. This is because the albedo measured in channel 2 due to vegetation elevates the channel 2 over the channel 1 reflectance. The channel 2-1 reflectance difference solved the problem of land mistakenly being classified as lake or water.

The third step is to identify snow on the ground in trees. Selective scatter plots showed that the snow pack often was partially obscured by trees that lowered the channel 1 reflectance. The range of channel 1 reflectance was set to extend the high reflectance of unobscured snow to lower albedos to compensate for the snow in trees. Additionally the channel 3 - 4 temperature difference for snow was found to be consistently small from the scatter plots due to weak channel 3 reflectance. Therefore to be classified as a snow in trees pixel, the channel 1 reflectance was lower than that of open snow and but the channel 3-4 temperature difference remained nearly unchanged.

The fourth step is to identify snow. This is done by using the strong channel 1 reflectance coupled with the previously mentioned small channel 3-4 temperature difference to distinguish snow. The condition that the channel 2-1 reflectance difference must also be negative keeps mixed land pixels from being classified as snow.

The fifth step of the classification routine tests for snow free land. As with the lake pixels a low channel 1 reflectance is set for a threshold. Larger variations in the channel 3-4 temperature difference are found in the scatter plots for land than in lake pixels and this threshold is raised over the lake values. Again the channel 2-1 reflectance difference must be uniquely positive for a pixel to be classified as land.

The sixth step is to separate out cumulus or liquid type clouds by using a single threshold based on the channel 3 reflectance. As discussed in chapter two the channel 3 reflectance is estimated by subtracting channel 4 from channel 3. Surface scatter plots

show a very large channel 3 reflectance for liquid clouds. This feature of liquid clouds was thoroughly investigated by Allen (1987) and Barron (1988).

At this stage in the algorithm the major surfaces such as lake, land, high cloud, liquid cloud and snow have been segregated. A pixel that has not been classified at this point is either a cloud that did not fall into the high or liquid cloud category or a mixture of several surfaces. The algorithm now attempts to further distinguish these surfaces.

The seventh step of the routine makes a final attempt to identify clouds not previously classified. Since every surface pixel has been identified at this point in the algorithm, the single channel 4 temperature threshold can be raised without fear of falsely distinguishing cold surface features for clouds. A channel 1 reflectance is also set above that of snow free land to make certain that the pixel is bright as well as cold.

Finally the last step is to assign a gray shade to a pixel that has failed to be classified. This type of pixel is a mixed pixel with various surface concentrations that allude all thresholds.

C. PROCESSING SSM/I DATA

The microwave data used for this study was acquired from the Cooperative Institute for Research in Environmental Sciences (CIRES) National Snow and Ice Data Center. This data was geographically centered over the Great Lakes and the West Coast regions of the United States and Canada. The Great Lakes data set covered the same geographic location as NOHRSC windows seven and nine on 30 January through 21 February 1990. The West Coast data coincided with NOHRSC windows one, two and 12, and included sections of window three and four during 13 February through 24 March 1990. This data included the 19, 22, 37 and 85 GHz channels. As mentioned previously only the

horizontally polarized segment of the 85 GHz channel was usable from this data set due to spacecraft sensor failure.

The data was received in nine track format and loaded into the VAX computer where selected files were processed. Program SSMI_MAP converted the temperature data to a 512 by 512 image using a conical equal distance projection. SSMI_MAP performs nearest neighbor interpolation to fill the map as needed at high resolutions. Low resolution images do not require any gap filling and are not interpolated. Once the images have been mapped they are the same size regardless of frequency and can be directly compared and differenced.

The images were converted back to temperature data using program IMAGE_TO_REAL. As with the AVHRR data, once each pixel was assigned a brightness temperature various frequency combinations were graphed as scatterplots using program GET_DATA and NCAR graphics. Individual surfaces such a snow, land and water were then examined using programs SURVEY and GET_ASCII to create scatter plots. Program CLASSMIU used these graphically derived thresholds to create a new, classified composite image.

1. SSM/I Separation Algorithm

The SSM/I separation algorithm was developed from three subscenes taken from the Great Lakes data set on 2 February, 11 February and 20 February, 1990. Approximately 25 scatter plots were made for each case to determine thresholds. Figure 3.5 shows the bi-spectral combinations of frequencies and frequency differences used for this study. Temperature thresholds for snow, land and water were established for 37V GHz, 37H GHz and 85H GHz channels. Also examined was the 37 GHz polarization temperature difference and the 85H GHz minus the 37H GHz temperature difference for each surface.

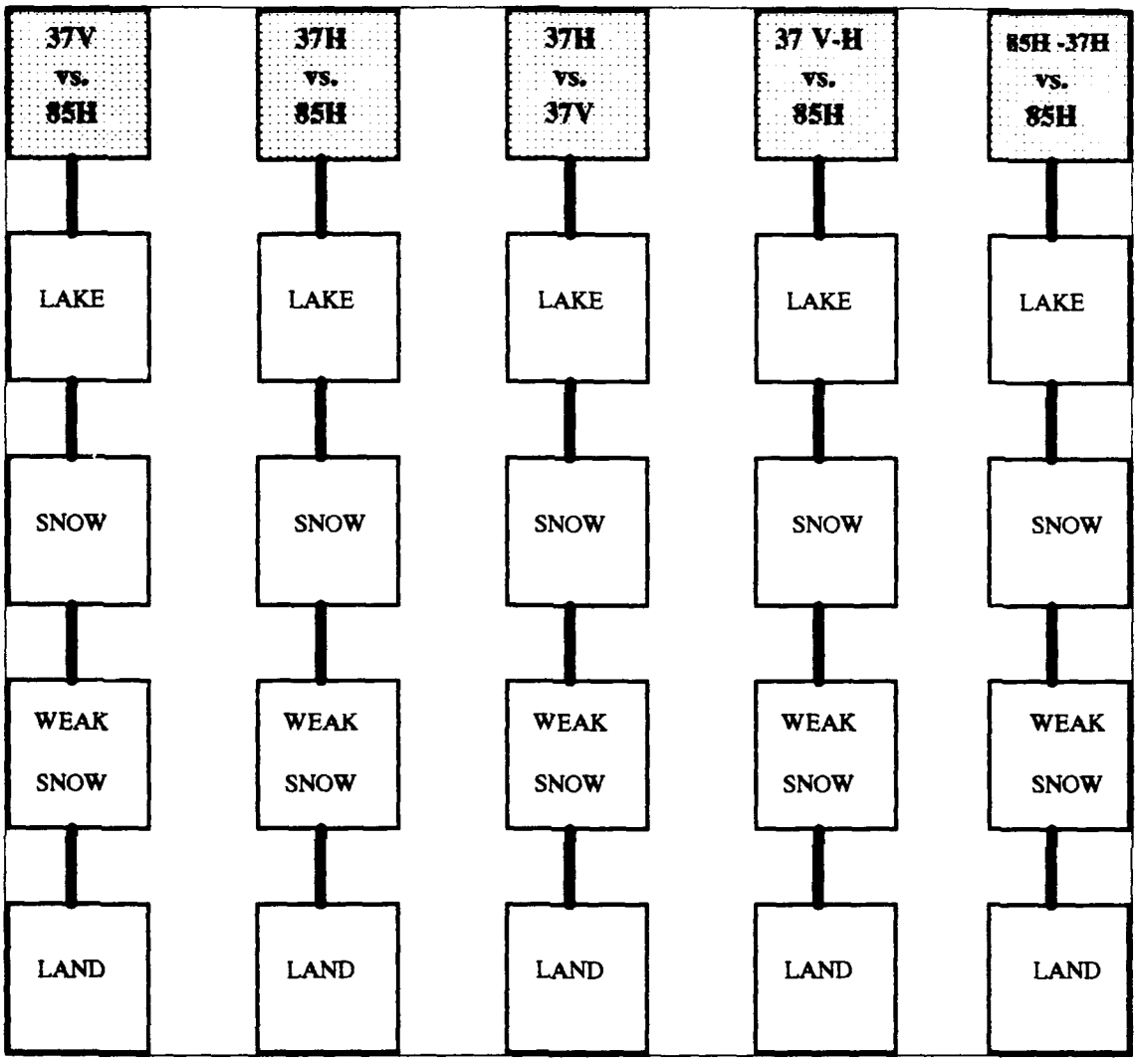

Figure 3.5 - Family of SSM/I scatterplots.

As with the AVHRR images, a separation algorithm was written that uses the temperature thresholds to construct a separated composite image of known gray shades. Again a logical block-if statement moves from pixel to pixel location and determines if the data associated with a given pixel falls into a selected range necessary for classification. Five 512 by 512 data arrays are read into the algorithm and give each pixel location a specific identity which may or may not fall into a selected threshold range

necessary for classification. The arrays used are the 37V GHz brightness temperature, the 37H GHz brightness temperature, the 85H GHz brightness temperature, the 85H minus the 37H GHz brightness temperature and the 37 GHz polarization temperature difference. Figure 3.6 shows a schematic of the data arrays assigned to each pixel location.

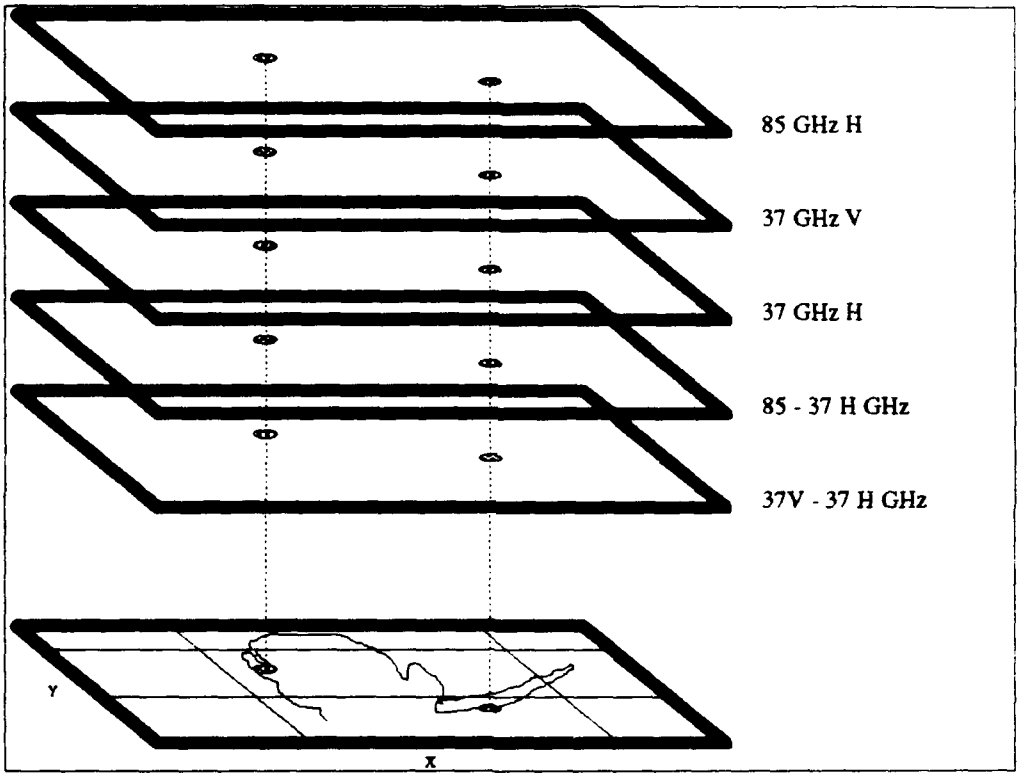

Figure 3.6 - Stacking of the 512x512 data arrays in program CLASSMI.

The logical block-if segment of the separation algorithm is composed of 18 statements. Figure 3.7 illustrates the decision process used for surface separation. Although there are more steps to this algorithm than the AVHRR separation algorithm, it is actually a simpler routine. Each step in the SSM/I algorithm is strictly bi-spectral and essentially sets horizontal and vertical limits or thresholds derived from the two

dimensional scatter plots. Five different frequency combinations are used to express each surface with slightly different thresholds. Any one statement that is found to be true results in a pixel being classified.

IF 37V vs. 85H LAND THRESHOLDS IN RANGE
(37V: 250-274 K, 85H: 247-274 K)
OR
IF 37H vs. 85H LAND THRESHOLDS IN RANGE
(37H: 247-263 K, 85H: 247-274 K)
OR
IF 37V vs. 37H LAND THRESHOLDS IN RANGE
(37V: 250-274 K, 37H: 247-263K)
OR
IF 37V-37H vs. 85H LAND THRESHOLDS IN RANGE
(37D: 0-10 K, 85H: 247-274 K)
OR
IF 85H-37H vs. 85H LAND THRESHOLDS IN RANGE
(85-37H: 0-25 K, 85H: 247-274 K)
THEN
LAND

ELSE
IF 37V vs. 85H SNOW THRESHOLDS IN RANGE
(37V: 224-247 K, 85H: 184-225 K)
OR
IF 37H vs. 85H SNOW THRESHOLDS IN RANGE
(37H: 187-225 K, 85H: 184-225 K)
OR
IF 37V vs. 37H SNOW THRESHOLDS IN RANGE
(37V: 224-247 K, 37H: 187-225 K)
OR
IF 37V-37H vs. 85H SNOW THRESHOLDS IN RANGE
(37D: 5-50 K, 85H: 184-225 K)
OR
IF 85H-37H vs. 85H SNOW THRESHOLDS IN RANGE
(85-37H: - 50-0 K, 85H: 184-225 K)
THEN
SNOW

Figure 3.7 A - Program CLASSMIU decision path.

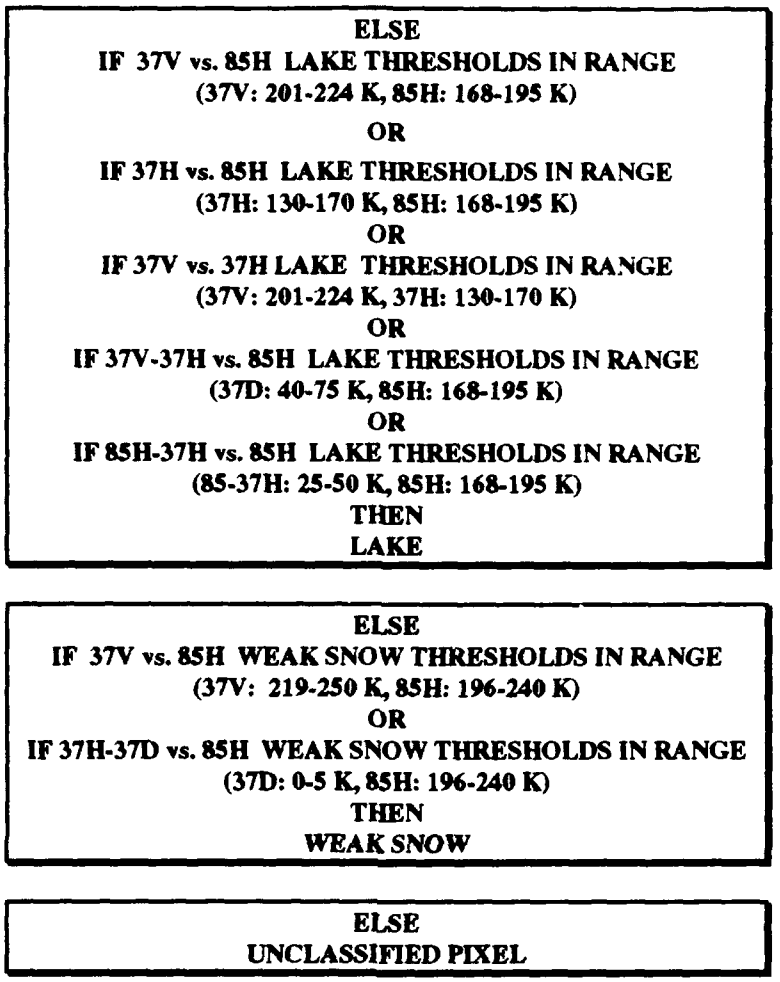

Figure 3.7 B - Program CLASSMIU decision path (continued).

Steps one through five test each pixel for snow free land. The brightness temperatures associated with land were the highest of any surface observed on the images and relatively small positive temperature differences were found in the polarization and multi-channel differencing. The bi-spectral combinations tested are 37V versus 85H GHz, 37H versus 85H GHz, 37H versus 37V GHz, 85H minus 37H versus 85H GHz and 37v minus 37H versus 85H GHz.

Steps six through ten check for snow. Scatter plots showed that snow typically had brightness temperatures that fell between the warm land and much colder water. Polarization differences were noted in the snow pack as reported by McFarland *et al.* (1987). Also noted was a negative 85H minus 37H GHz temperature difference in the presence of snow. This is likely due to the fact that the volume scattering of the snow attenuates the 85h GHz signal more strongly than the 37 GHz signal. The five steps to identify snow have the same frequency combinations as those used to test for land.

Steps 11 through 15 test the pixel location for lake characteristics. Lake brightness temperatures are colder than any found on the microwave image with 37H GHz being the coldest. Very large 37 GHz temperature differences as well as large 85H minus 37H temperature differences were found in the scatter plots. These cold temperatures and temperature differences were used to classify the lake and ocean pixels.

Steps 16 and 17 were added after test of the algorithm showed that large areas of the image were not being classified. Comparisons with the AVHRR imagery revealed that the unclassified areas were regions of snow covered land that did not have the proper thresholds to be classified as snow. In the AVHRR image these areas often appeared as snow in trees or snow with a lowered channel one reflectance caused by thin snow. This category is labeled as weak snow and uses thresholds set in the 85H, 37V and the 37V *minus* 37H GHz frequencies. Finally, as with the AVHRR routine, any pixel that fails to get classified is assigned a gray shade and can be identified as an unclassified pixel.

IV. RESULTS

A. GREAT LAKES REGION

The Great Lakes region served as an algorithm development area for both the AVHRR and SSM/I imagery. A total of six AVHRR 512 by 512 subscenes were taken from NOHRSC Window nine. Two subscenes were from 31 January, two from 11 February and two from 20 February, 1990.

The parallel SSM/I imagery was selected to coincide as closely as possible to the AVHRR imagery spatially and temporally. Below 50 degrees north latitude complete coverage of the ground by SSM/I is not available on a daily basis. This meant that in several cases the AVHRR and SSM/I data were separated by time spans of 24 hours or greater. These temporal differences have been noted in the individual case analyses. The dates selected for the comparative SSM/I imagery were 30 January and 2 February which corresponded to the AVHRR imagery from 31 January 1990. SSM/I images were also studied from 10 February and 11 February to match the 11 February 1990 AVHRR images. The final Great Lakes microwave imagery was selected from 20 February to match the AVHRR imagery from 20 February 1990.

1. Case 1

Case 1 AVHRR Data was taken from 1902 GMT 31 January and was broken into a west and east 512 by 512 subscene. Figures 4.1 and 4.2 show the two subscenes from channel 1. Figure 4.1 is centered near London, Canada which is situated between Lake Huron and Lake Erie. Figure 4.2 has its center near the Adirondack Forest of New York.

Figure 4.1 - 31 January west AVHRR channel 1 subscene.

Figure 4.2 - 31 January east AVHRR channel 1 subscene.

Surface analyses indicate that a low pressure center, located in northern New Jersey on the 0300 GMT 30 January surface plot, was providing snow from the western edge of Lake Erie through upstate New York. The 0000 GMT 1 February surface analysis plot shows temperatures above freezing in central Michigan south of Saginaw Bay and temperatures below freezing to the north of the Bay. In eastern upstate New York temperatures were holding at, or slightly below freezing.

Figures 4.3 and 4.4 show the AVHRR and SSM/I algorithm produced composite images of the same location as figure 4.1. In the AVHRR composite image, figure 4.3, brown represents snow free land, white a strong snow signal and gray a weaker snow signature. Magenta represents high cloud, yellow represents liquid cloud and pink shows cloud that falls between these two categories. Blue is assigned to pixels believed to be water and red is given to any pixel that remains unclassified by the algorithm.

Snow is distinctly seen in figures 4.1 and 4.3 north of Saginaw Bay, Michigan with the snow line extending to the southwest. Snow free land is found south of Saginaw Bay to the western tip of Lake Erie where a second snow line extends to the southwest. The existence of the snow lines agree with the temperatures shown in the surface plots. The line of blue pixels between the snow and snow free land in central Michigan is believed to be due to melting snow. Unclassified pixels (red) exist along the borders of distinct surfaces as well. They represent pixels of a distinct or mixed surface that are not classified by a threshold in the algorithm contained in program CLASSIFU. Red pixels are seen at some urban locations such as Detroit or Lansing, Michigan, particularly when the cities are surrounded by snow. This is because the channel 2 reflectance is lowered in metropolitan areas as a result of man made structures and less extensive vegetation. The channel 2 minus channel 1 reflectance difference is negative making the pixels fail the requirement necessary to be classified as land.

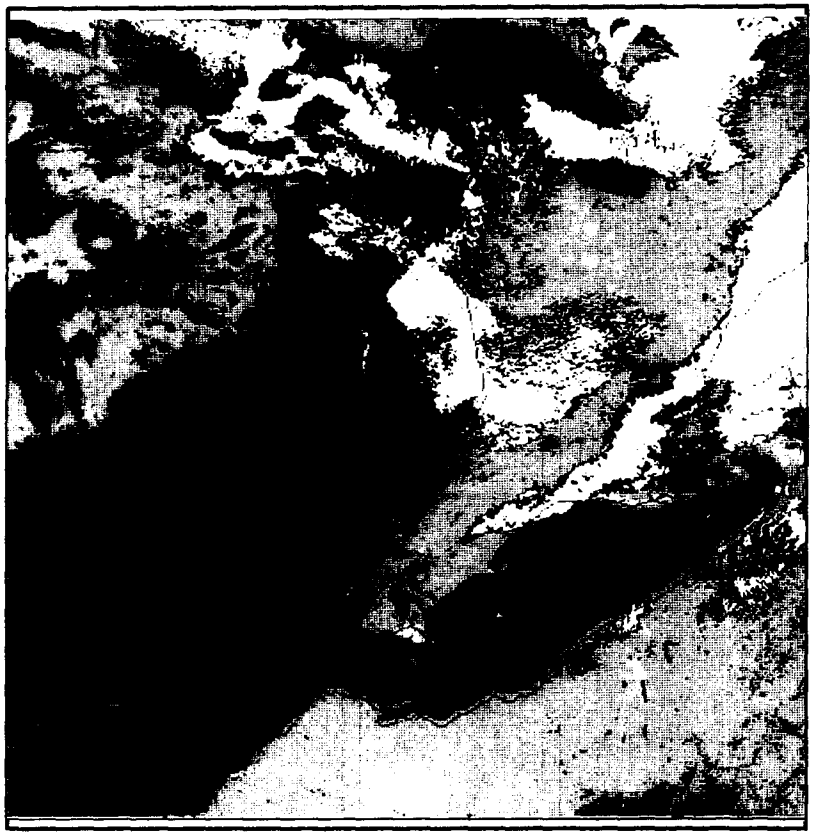

Figure 4.3 - 31 January west AVHRR composite subscene.

Figure 4.4 - 30 January west SSM/I composite subscene.

There was no exact SSM/I match for the AVHRR data on 31 January. Both SSM/I passes available from that date covered very small portions of the AVHRR image. Good coverage was obtained on 30 January at 1021 GMT which was approximately 33 hours before the AVHRR pass. This SSM/I pass only spatially matched the AVHRR images in figures 4.1 and 4.3 as coverage from this satellite pass extended just to the eastern edge of Lake Erie. Figure 4.4 shows the composite image created from program CLASSMIU at the same general location as the AVHRR data. The AVHRR images and SSM/I images are not mapped using the same projection so there is not a one to one match in pixel locations. In the SSM/I composite image brown represents snow free land and blue represents water. A strong snow signature is colored as a white pixel while a weaker snow signal is seen as a gray pixel. Unclassified pixels from the algorithm are colored red.

The position of the snow line in northern Michigan in figure 4.4 appears to match very closely to the snow line seen in figure 4.3. Snow is also seen to the east across Lake Huron in both the SSM/I and AVHRR images. The snow lines east of Lake Huron in the images do not match up precisely and no snow can be seen south and west of Lake Erie in figure 4.4. It is difficult to determine from historic records if the snow not seen in the SSM/I imagery was on the ground at the time of the pass but the surface plots indicate that snow did fall on 29 and 30 January. It is likely that the separation algorithm is not sensitive to the brightness temperature and thickness of this snow cover.

Lake Erie is incorrectly classified as strong and weak snow instead of water. Additionally, a large portion of the lake is not separated into a distinct surface by the algorithm as indicated by the red colored pixels. The SSM/I algorithm consistently classified the boundaries of all major bodies of water as strong or weak snow. This is because in the pixel locations of land and water boundaries, the warm microwave

brightness temperatures of land transition to the cold brightness temperatures of water. The brightness temperature thresholds set for snow, which always fall between those set for land and water, are inevitably satisfied resulting in the snow classification. The significant horizontal extension of this erroneous snow is due large footprint size of the 37 GHz data. The large number of red pixels in the lake is likely due to the presence of precipitating clouds or lake ice, which have warmer brightness temperatures than the water and raise the pixel temperatures so that distinct surface thresholds are not met. If the signature of the clouds are sufficiently warm or the areal extent of ice is large, lake pixels are classified as snow.

Significant cloud cover is seen in figure 4.5, the right AVHRR composite image. Roughly 50 percent of this image is obscured by clouds which overlie the snow pack in many locations and are difficult to distinguish from snow in the channel 1 image. Clouds obscure Lake Ontario as well, but snow can be seen along the southern and northern shores of the lake between the clouds. The Finger Lakes of New York are observable as is a segment of the Hudson River which can be seen in the southeastern section of the classified image. Snow can be seen throughout New York, Vermont, Massachusetts, New Hampshire and Canada.

A second SSM/I image, figure 4.6 was analyzed from 2 February, approximately 34 hours after the AVHRR satellite pass. This imagery had good spatial agreement with figure 4.5. The snow line south of the Finger Lakes of New York has retreated to north of Lake Ontario and extends to the east coast of North America in Canada. This snow line position is considerably further north than seen in figure 4.5, the classified AVHRR imagery from 31 January. Synoptic charts for the period between the passes indicate a southerly flow of above freezing temperatures into the region which could account for the retreat of the snow line to the north. This would only be possible if the snow seen in the

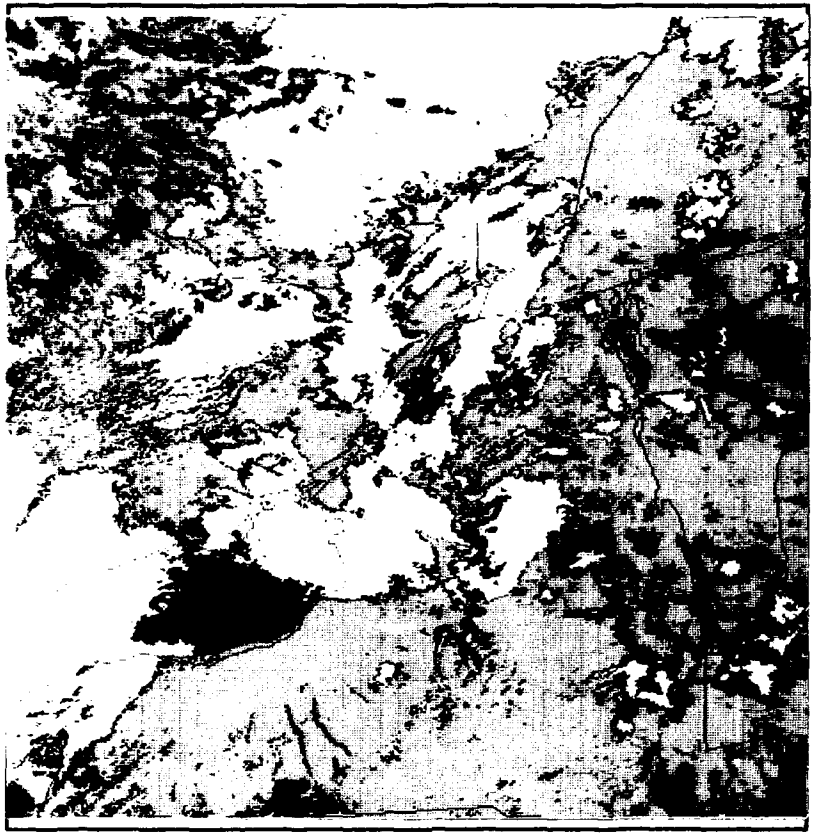

Figure 4.5 - 31 January east AVHRR composite subscene.

Figure 4.6 - 2 February east SSM/I composite subscene.

AVHRR imagery was very thin and susceptible to a quick melt off. It is also possible that the algorithm is not sensitive to the snow that may have been found on the ground at that time.

Lake Ontario is incorrectly classified as strong and weak snow and contains no water pixels. As with Lake Erie, the land and water boundaries are classified as snow because of the brightness temperature transition found at this interface. The unclassified pixels are likely a result of precipitating clouds which overlie the lake.

2. Case 2

Case 2 covers the same approximate geographic area as Case 1 but the AVHRR imagery is extracted from 1844 GMT 11 February 1990. Figure 4.7 shows the west channel 1 AVHRR image and figure 4.8 is the east image. These images view the same approximate locations as figures 4.1 and 4.2 respectively.

Figure 4.9 is the AVHRR composite image of figure 4.7. Extensive cloud cover can be clearly seen in the composite image as indicated by the yellow, pink and magenta colors. Some ice can be observed in Lake Erie and Lake Huron. Snow is again seen extending out from under the clouds in Michigan north of Saginaw Bay. Additional snow is seen east of Lake Huron and north of Lake Ontario. Again this snow is partially obscured by cloud cover. Unclassified pixels are grouped along major surface transition zones, areas of mixed pixels or for single but unique surfaces that failed to be classified by the thresholds set in the algorithm.

Figure 4.10 is the closest temporal matching SSM/I image that contained coverage of the Michigan area. This pass is from 2335 GMT 10 February, approximately 19 hours prior to figure 4.7. Snow is seen in northern Michigan with a snow line extending from northern Saginaw Bay west to Lake Michigan. More snow is observed across Lake

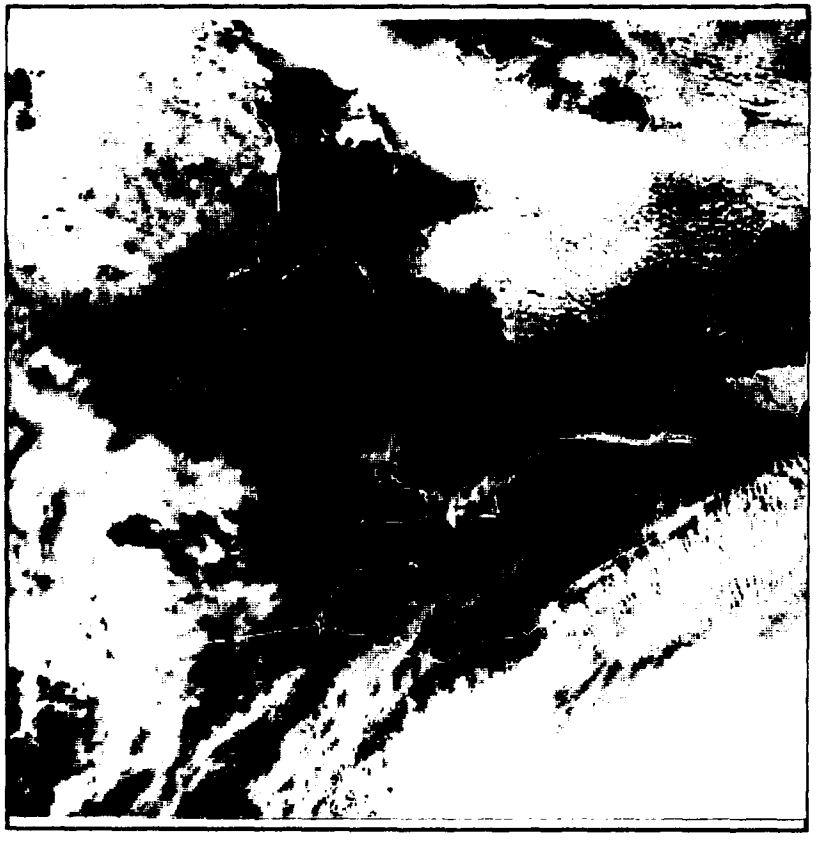

Figure 4.7 - 11 February west AVHRR channel 1 subscene.

Figure 4.8 - 11 February east AVHRR channel 1 subscene.

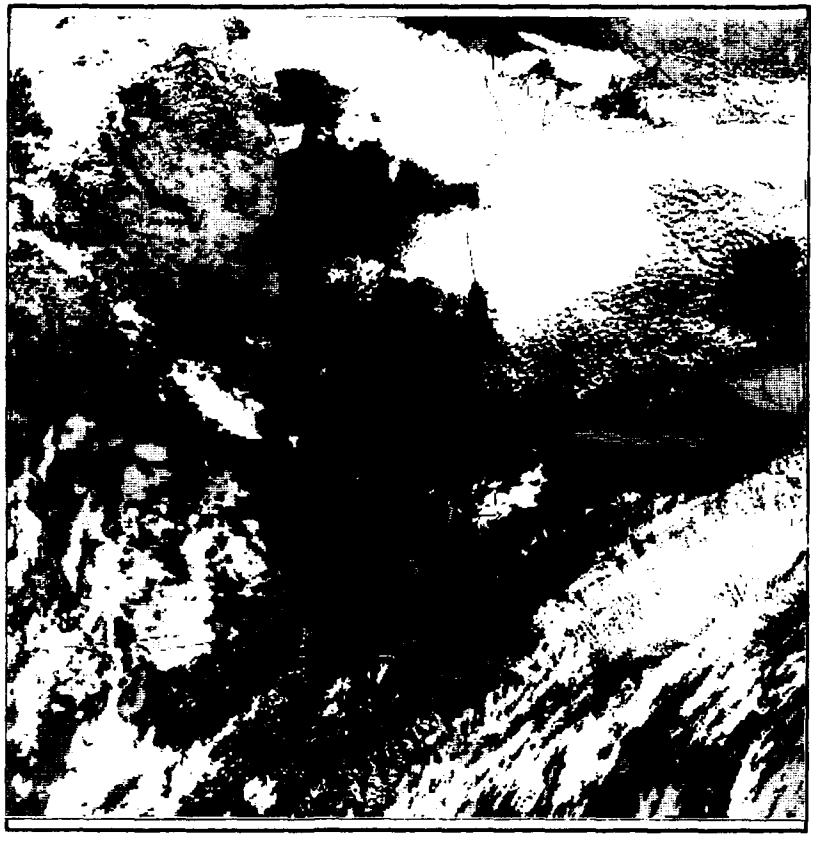

Figure 4.9 - 11 February west AVHRR composite subscene.

Figure 4.10 - 11 February west SSM/I composite subscene.

Huron south of Georgian Bay and north of Lake Erie. Both of these snow covered regions have excellent agreement with the classified AVHRR image seen as figure 4.9.

Lake Erie is correctly classified as water in this imagery as compared to the incorrect classification in Case 1. Again, the border of the lake is segregated as snow due to the brightness temperature transition that occurs at this boundary. The accurate classification of water pixels indicates that there are no precipitating clouds present.

Figures 4.11 and 4.12 are views of the same general location as figure 4.2. Figure 4.11 is the classified composite AVHRR image of figure 4.8. Bodies of water are strongly identified in this image. The Finger Lakes are clearly seen south of the cloud covered Lake Ontario. The Hudson River can also be seen originating from the New York City area which shows itself by being unclassified. Snow is found near the Finger Lakes and extends to the east across the Hudson River and into Massachusetts and Vermont. Snow is also seen throughout the image to the north of this line although a large portion of the image is covered by cloud.

In the northern areas of this image snow and land is intermixed which could be attributed to thin snow cover. This is a difficult assumption because many locations on the image are very heavily covered by trees. The darkening of the albedos by trees makes the identification of snow in trees difficult. There are also large areas of standing water seen north of Lake Ontario which indicate the possibility of melting snow. Temperatures recorded on the 11 February surface plot at 1800 GMT are hovering slightly below the freezing mark and contradict this idea. Extremely cold temperatures would indicate that the algorithm was incorrectly separating water pixels but temperatures near freezing make a performance assessment of the algorithm difficult. Other known lake and river locations in the images are classified correctly.

Figure 4.11 - 11 February east AVHRR composite subscene.

Figure 4.12 - 11 February east SSM/I composite subscene.

The best SSM/I temporal match for the AVHRR imagery is taken from an 0116 GMT 11 February 1990 satellite pass which was approximately 17 hours prior to the AVHRR pass. Only the AVHRR subscene over New York is imaged in the SSM/I pass. Figure 4.12 shows the classified SSM/I image that matches the same approximate area as figure 4.8. Snow can be seen extending east and south off of Lake Ontario, wrapping around the Adirondack Forest. No snow is observed in the forest itself and this oval area is colored brown as snow free land. It is impossible to observe this region in the AVHRR image because it is obscured by clouds. Snow can be seen east of the Hudson River in the AVHRR image and this is not detected by the SSM/I algorithm. Snow to the north of Lake Ontario and along the St. Lawrence valley is seen in both images.

3. Case 3

Case 3 covers the same geographic regions examined in Cases 1 and 2 on 20 February 1990. A major winter storm had swept across the northern Midwest through New England resulting in significant snowfalls on 16 and 17 February. The eastern half of the United States was under the influence of a large high pressure system on 20 February which provided an excellent opportunity for AVHRR imagery of ground features. Figure 4.13 covers the same geographic area as figure 4.1 showing the channel 1 image of the west subscene of the AVHRR satellite pass. Figure 4.14 is the east AVHRR channel 1 subscene of this same pass. The imagery from this AVHRR pass was taken at 1848 GMT.

Figure 4.15 is the AVHRR composite image of figure 4.13. Snow cover dominates both of these images and a very strong snow line extends along the Michigan and Ohio border to the western edge of Lake Erie. In both the channel 1 and classified images the snow line is very distinct and sharp. Unclassified pixels can be seen in surface border locations as well as in larger metropolitan areas such as Detroit, Flint,

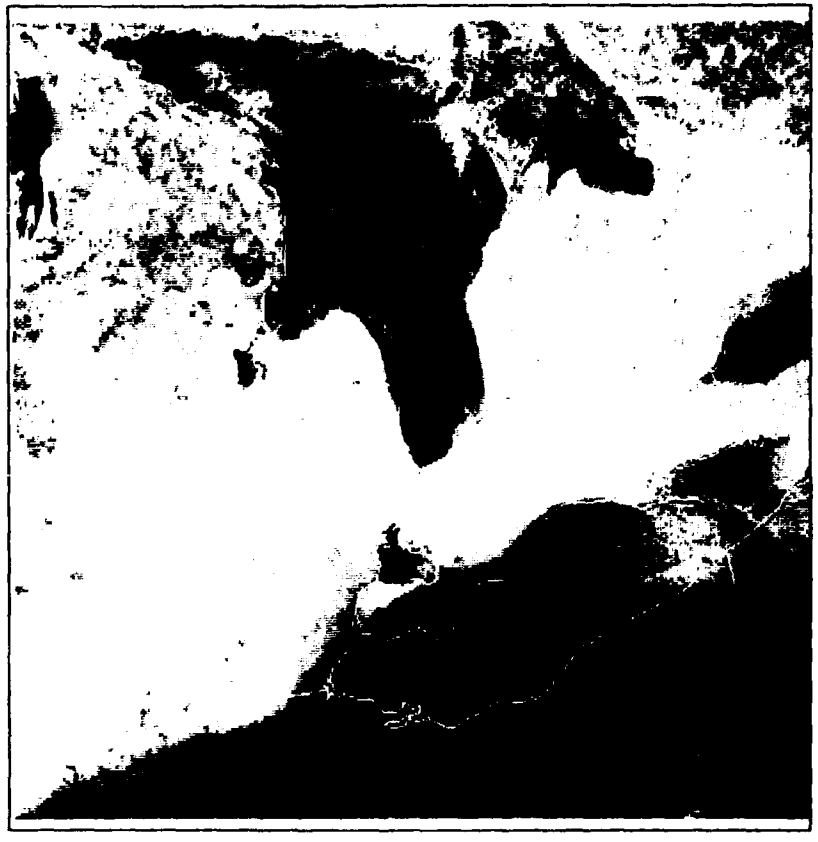

Figure 4.13 - 20 February west AVHRR channel 1 subscene.

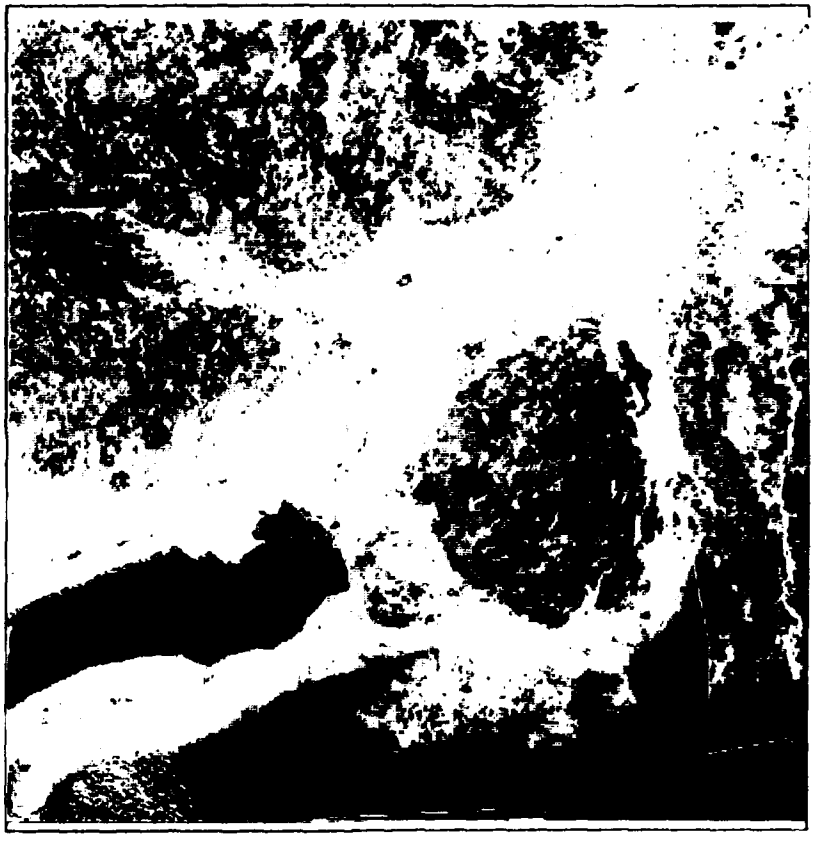

Figure 4.14 - 20 February east AVHRR channel 1 subscene.

Saginaw and Lansing, Michigan. Except for a band of cloud stretching from Lake Huron to eastern Lake Erie, the image is cloud free. Ice can be seen in Lake Huron, Georgian Bay and Lake Erie.

Figure 4.16 is the classified SSM/I image from 1225 GMT 20 February, approximately six hours prior to the AVHRR pass. The time interval between passes and the agreement of areal coverage between the two satellites was the best of any case studied in the Great Lakes region. Only a small portion of western Michigan was missed in this pass making it an excellent comparative image with the AVHRR scene. Figure 4.16 shows a nearly identically positioned snow line along the Michigan and Ohio border as seen in the AVHRR image 4.15. The snow line appears to extend below Lake Erie, but this presence of snow pixels is observed at every land and water interface.

Figures 4.17 and 4.18 represent the AVHRR and SSM/I classified composite images of same geographic area covered by image 4.14. In figure 4.17 a distinct snow line can be seen south of Lake Ontario which becomes less pronounced south of the Adirondack Forest and east toward Vermont. Trees confuse the separation algorithm in the Adirondack Forest and keep the albedo low enough to have some of the pixels in this area labeled as snow free land. Areas to the north of the St. Lawrence Seaway between Quebec and Montreal are contain very thick forests making the classification of snow in this area very difficult and again some pixels are classified as snow free land. Several cumulus type clouds can be seen as yellow pixels in the upper northeast corner of the image. These clouds are located over the snow pack and can be barely seen in the channel 1 image.

Figure 4.18 shows the SSM/I parallel image to figure 4.17 which was extracted from the same SSM/I pass as figure 4.16, six hours prior to the AVHRR pass. The areal extent of snow is in excellent agreement with AVHRR composite figure 4.17. It is

Figure 4.15 - 20 February west AVHRR composite subscene.

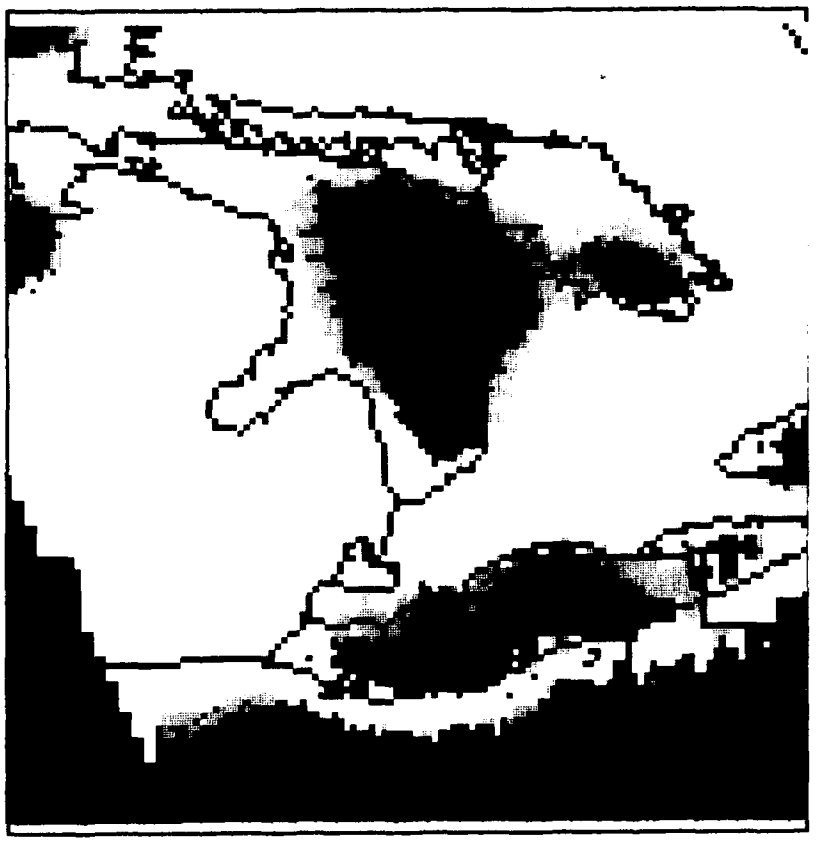

Figure 4.16 - 20 February west SSM/I composite subscene.

Figure 4.17 - 20 February east AVHRR composite subscene.

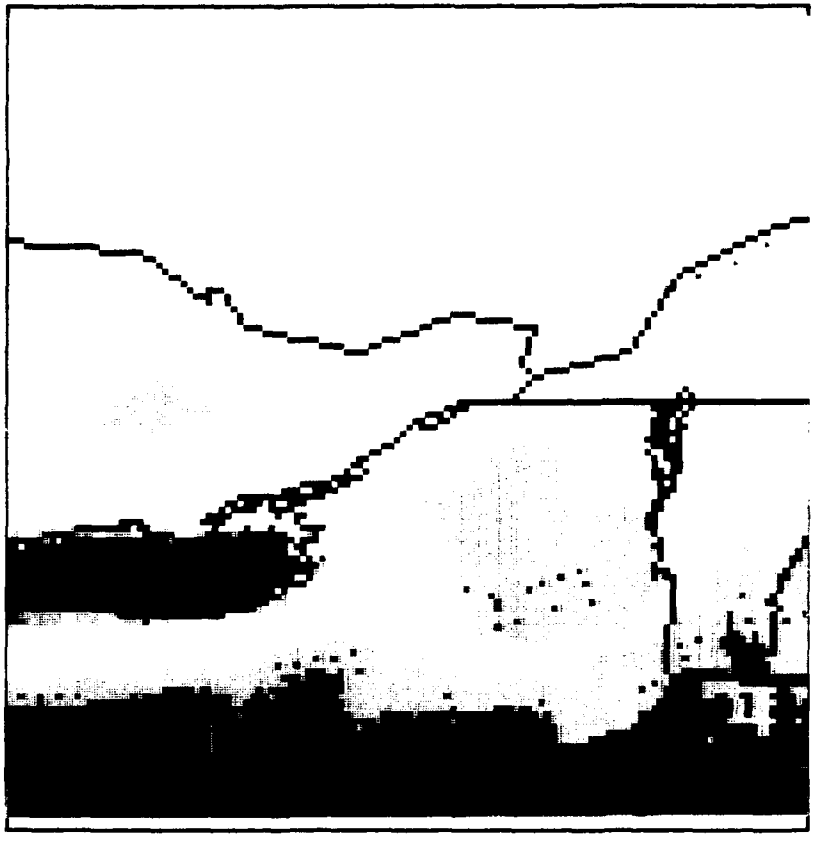

Figure 4.18 - 20 February east SSM/I composite subscene.

particularly interesting to note that the outline of the Adirondack Forest can be seen with the stronger snow signature snow (white) wrapping around the weaker snow signature (gray). In contrast with Case 2 a weak snow is now seen in the forest. Unlike the AVHRR image, a strong snow signature is seen throughout the image north of the snow line. A weaker snow signal is observed north of Lake Ontario in the region of Algonquin Provincial Park which is another region that has dense forests.

B. WESTERN UNITED STATES REGION

The second data set examined covered an area that included all of California, Oregon, Washington and Idaho as well as sections of Montana, Wyoming, Utah and Arizona. A total of six AVHRR 512 by 512 subscenes were examined from NOHRSC windows one and two. Three subscenes were taken from NOHRSC region one and three subscenes from region two on 14 February, 26 February and 15 March, 1990.

The western AVHRR data tested the AVHRR algorithm in a new region of the United States that included more vertical terrain. The algorithm required two modifications to reduce the number of incorrect and unclassified pixels. The channel 1 reflectance thresholds set for land separation had to be raised to allow desert sand, with a high albedo, to be classified. Also the channel 4 brightness temperature threshold set for high cloud had to be lowered so that cold mountain tops would not be segregated as high cloud.

SSM/I imagery was again selected to match the AVHRR imagery spatially at as close a time interval to the AVHRR passes as possible. This data was taken from satellite passes flown on 14 February, 27 February and 15 March,1990. All of the SSM/I images examined for comparison with the parallel AVHRR images were from night time passes.

In all cases the temporal spacing between the AVHRR and SSM/I data was less than 24 hours and the areal coverage of the two data sets was in complete agreement.

1. **Case 4**

Case 4 covers two separate regions taken from AVHRR NOHRSC window one and window two on 14 February 1990. The window one imagery, shown in channel 1 as figure 4.19, is a subscene centered over the Snake River Valley of Idaho. The second channel 1 AVHRR subscene is taken from window two and is centered near Round Mountain, Nevada with the Sierra Nevada Mountain Range imaged to the west.. This subscene is shown as figure 4.20. The time of the window one pass was 2136 GMT and the window two pass was 2134 GMT.

On 12 and 13 February a cold front, that stretched from northern Idaho through northern California, had pushed south bringing snow and snow showers to some areas of northern Utah and Nevada. Heavier snow was reported falling near Sun Valley, Idaho on 14 February according to the 0100 GMT weather depiction chart. Clear skies were shown for most of northern California and southwestern Idaho at 1900 GMT, two and one half hours prior to the AVHRR satellite pass.

Figures 4.21 and 4.22 are the respective AVHRR and SSM/I classified composite images that correspond to figure 4.19, the window one Idaho subscene. The time of the SSM/I pass was at 0356 GMT on 14 February, approximately 18 hours prior to the AVHRR satellite pass. In figure 4.21 cloud cover is depicted along the Nevada and Idaho border as well as to the north, along the Washington and Idaho border. The Great Salt Lake in Utah is seen sandwiched between liquid type clouds (yellow) and higher, colder clouds (pink and magenta). Additional water can be observed in sections of the Snake River Valley. Snow covers the southwest corner of Idaho and extends into Oregon

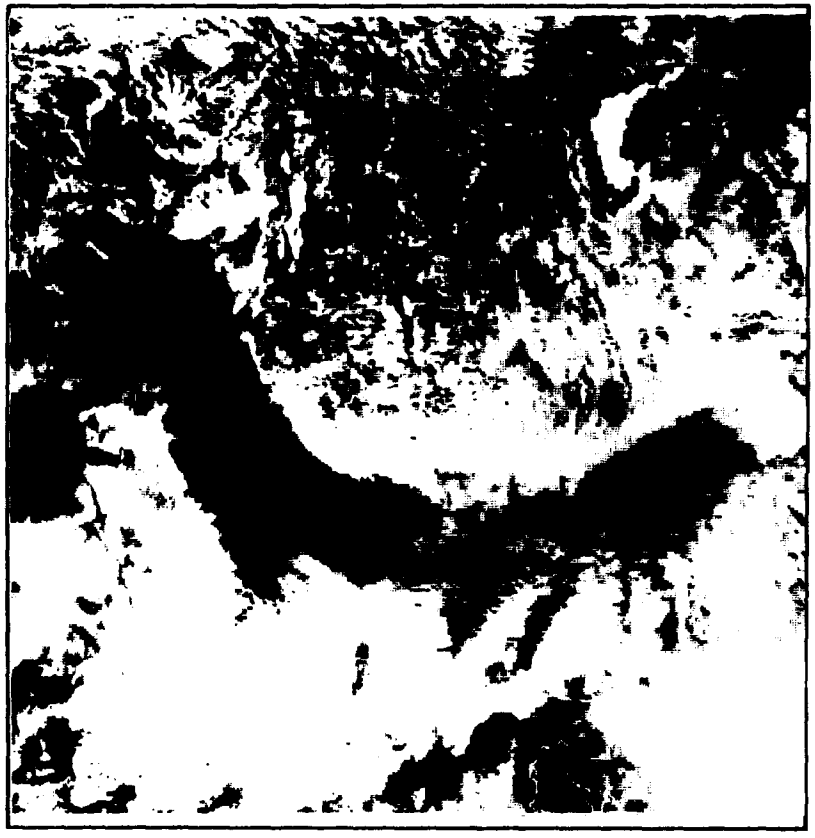

Figure 4.19 - 14 February AVHRR channel 1 window one subscene.

Figure 4.20 - 14 February AVHRR channel 1 window two subscene.

Figure 4.21 - 14 February window one AVHRR composite subscene.

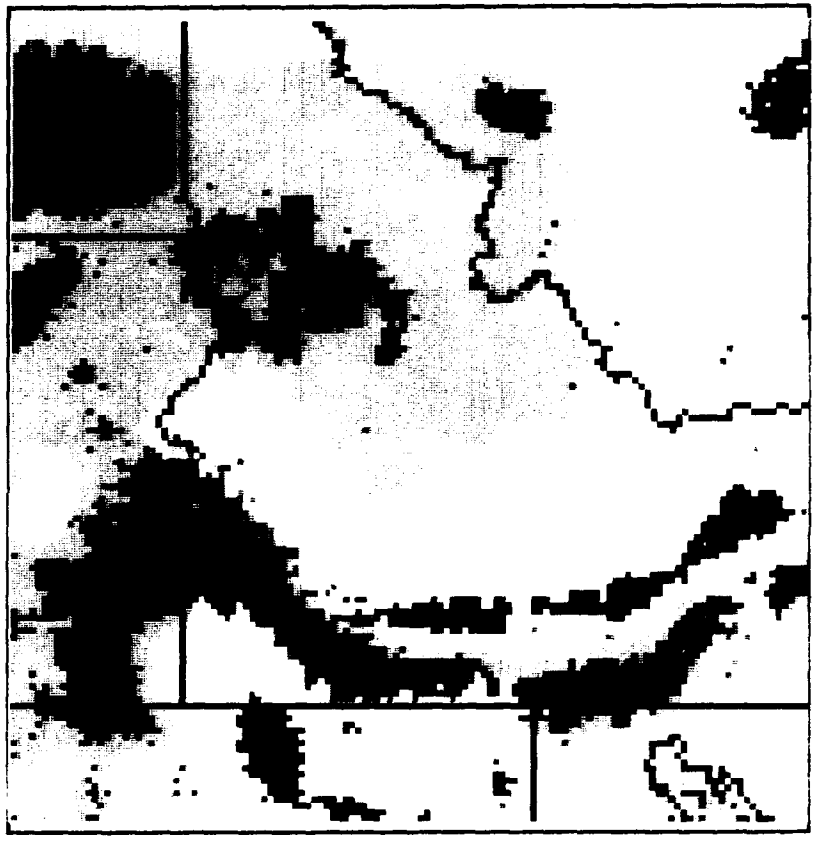

Figure 4.22 - 14 February window one SSM/I composite subscene.

and Nevada. Snow is also seen in the mountains north of the Snake River Valley as well as to the east of the valley toward the Wyoming border.

The comparison SSM/I image, figure 4.22, shows extensive snow coverage throughout the subscene. The curving Snake River Valley is a striking feature in this image as well as figure 4.21. For the most part, the valley is classified as snow free land. South of the Snake River Plain, the areal extent of snow is in general agreement with the AVHRR image except for the area around the Great Salt Lake. Snow is indicated in this region in figure 4.22 but is not seen in figure 4.21, the AVHRR composite image. It is possible that the microwave signature of the salt flats that surround the Great Salt Lake to the north through southwest is depressed below that of typical snow free land and makes this area separate as snow covered land in the classification algorithm.

To the north of the Snake River Valley the snow patterns show agreement. A strong snow signal runs across the northern lip of the valley matching the snow edge in the AVHRR composite image. Snow also extends into Oregon in both images. An area of disagreement exists in the right center of the images north of the Snake River Valley where the AVHRR image shows snow free land and the SSM/I image shows a strong to weak snow signal. The sun angle and mountainous topography causes shadowing in the AVHRR image and lowers the albedo of the snow, forcing pixels to be separated as snow free land.

Figures 4.23 an 4.24 are the respective classified composite images of the window two AVHRR and SSM/I subscenes that include coverage of the Sierra Nevada Mountain Range. The SSM/I image is cut from the same pass as figure 4.22. Extensive cloudiness is seen to the east of the mountains over central Nevada in both the AVHRR channel 1 image and the classified composite image. The presence of clouds is also reported on the 1900 GMT weather depiction chart with three to four thousand foot AGL scattered to

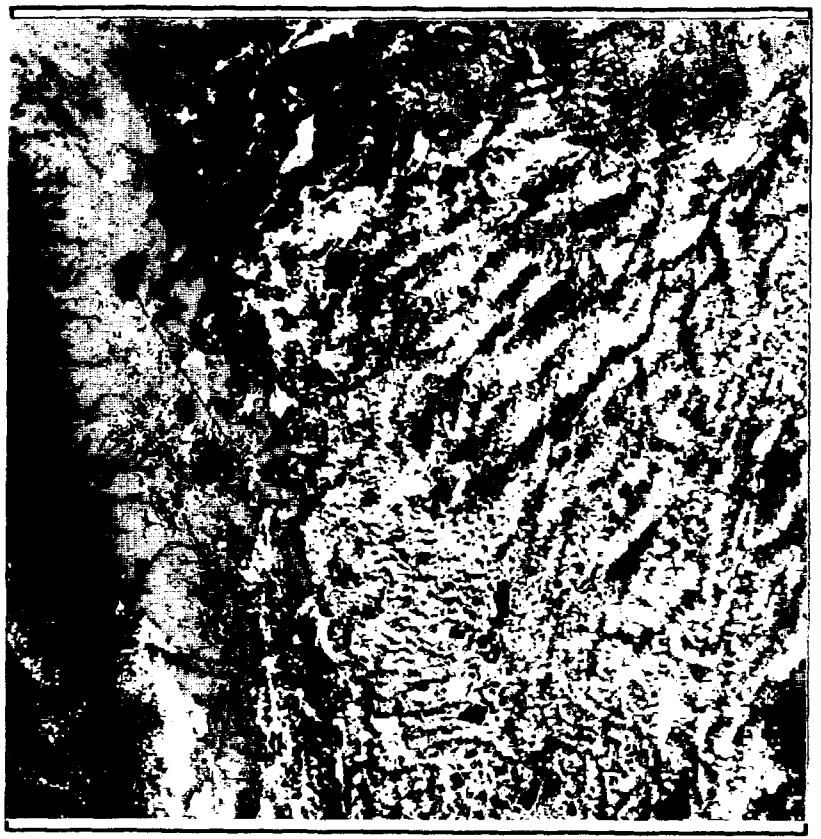

Figure 4.23 - 14 February window two AVHRR composite subscene.

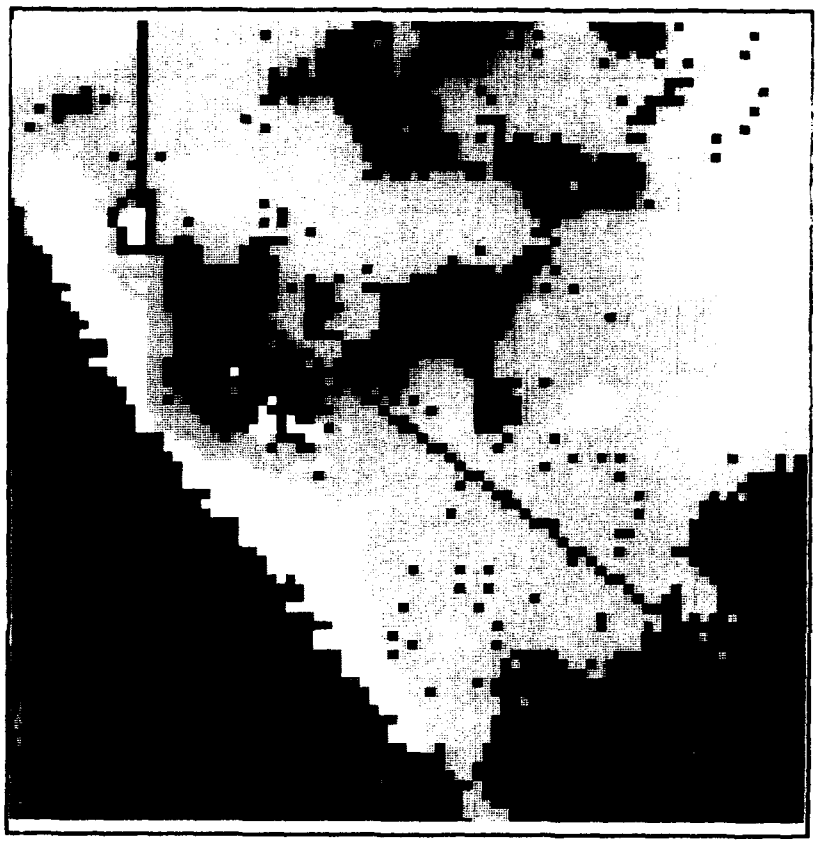

Figure 4.24 - 14 February window two SSM/I composite subscene.

broken cloud decks reported from all Nevada stations except Reno, which was reporting clear skies. These clouds are separated by the AVHRR algorithm as yellow pixels in figure 4.23. Snow is seen throughout the higher elevations of the Sierra Nevada Range and the results of the algorithm generated image appears in excellent agreement with the channel 1 image. Snow is also seen in the northeast corner of the image near the Idaho and Nevada border. Outstanding separation of the lakes in the mountains can be seen in the AVHRR classified image. Honey, Pyramid, Walker and Mono Lakes as well as lakes Tahoe and Almanor are distinctly seen as blue pixels.

The comparison SSM/I image to figure 4.23, figure 4.24, indicates that the areal extent of snow is more wide spread than indicated by the AVHRR images. The strong snow signal (white) seen in the mountains is in good agreement with snow seen in the AVHRR image but an additional weak snow signal (gray) is shown throughout most of Nevada. Although a large portion of this region is covered by broken clouds in the AVHRR image, it appears that little, if any, snow can be seen in areas not obscured by clouds. Extensive areas of unclassified pixels (red) are present in the classified SSM/I image indicating that the thresholds of the separation algorithm were out of range for a large number of pixels. It is believed that the actual land brightness temperatures were simply too cold to be classified as snow free land and many pixels were erroneously segregated as weak snow or left unclassified. Strong snow signatures (white) are in approximate agreement with snow observed in the AVHRR images.

2. Case 5

Case 5 covers the same geographic locations as Case 4 on 26 February 1990. The channel 1 AVHRR imagery is shown in figures 4.25 and 4.26 which represent the window one and window two subscenes, respectively. The time of the window one pass was 2108 GMT and the window two scene was 2106 GMT. No significant weather

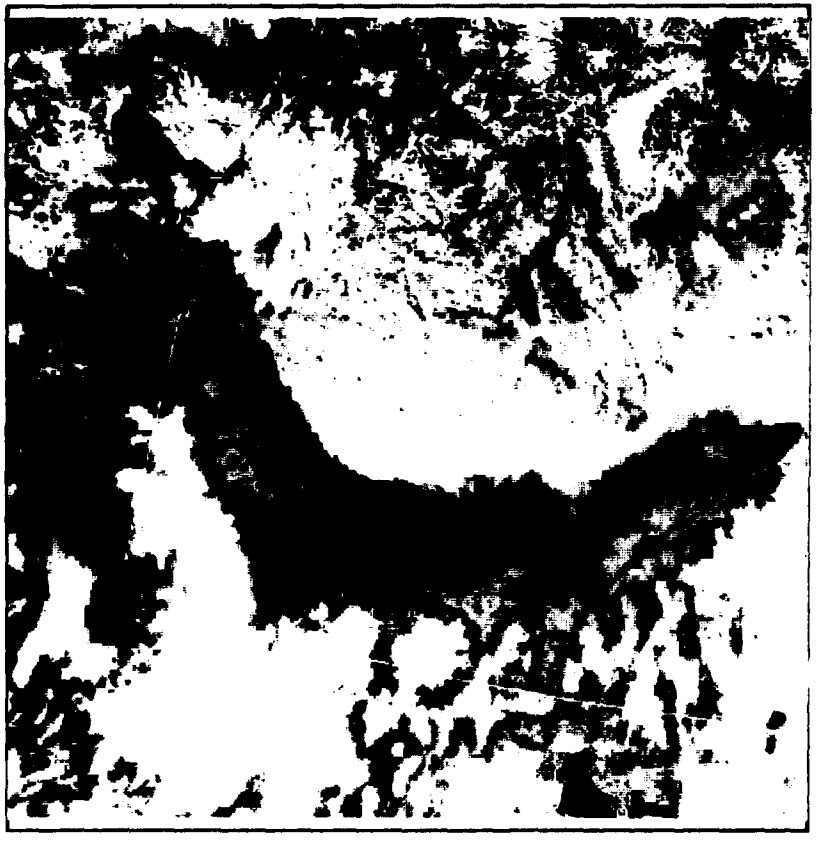

Figure 4.25 - 26 February AVHRR channel 1 window one subscene.

Figure 4.26 - 26 February AVHRR channel 1 window two subscene.

was indicated in the subscene locations for the week prior to the satellite passes on either the surface analysis plots or the weather depiction charts. The 1900 GMT weather depiction chart shows high broken to overcast cloud conditions at all Nevada reporting stations and 25,000 foot AGL scattered clouds in southern Idaho.

Figures 4.27 and 4.28 are the respective AVHRR and SSM/I classified composite images that match the figure 4.25 window one Idaho subscene. The SSM/I satellite pass occurred on 27 February at 0426 GMT, approximately seven hours after the AVHRR pass over the same location. Figure 4.25, the channel 1 AVHRR subscene, shows very thin cloud cover in northern Nevada and Utah. Somewhat thicker clouds are noticeable north of the Snake River Valley. These clouds are generally not classified because they are too thin and exhibit characteristics of the underlying ground. The clouds do not meet the channel 3 reflectance thresholds and their channel 4 brightness temperature is too warm to be classified as high clouds. Some pixels of the cloud cover do have the proper channel 3 reflectance thresholds estimated by the channel 3 *minus* the channel 4 brightness temperature difference to be classified as liquid cloud (yellow).

Snow is seen on the northern and southern sides of the Snake River Valley in nearly an identical pattern as that observed in figure 4.21, 12 days prior to this satellite pass. Some snow has melted in the extreme southwest corner of Idaho as well as in Oregon and Montana. This melting snow appears to be imaged in the southwest corner of Idaho and can also be seen along the northern rim of the Snake River Valley and in the northwest corner of the subscene in eastern Oregon. The 2100 GMT surface analysis chart shows the Boise, Idaho temperature to be at 52 degrees Fahrenheit. The Great Salt Lake is clearly separated as is American Falls Reservoir in the Snake River Valley and Bear Lake, which lies exactly on the Idaho and Utah border and is partially obscured by clouds in the southeastern corner of the subscene.

Figure 4.27 - 26 February window one AVHRR composite subscene.

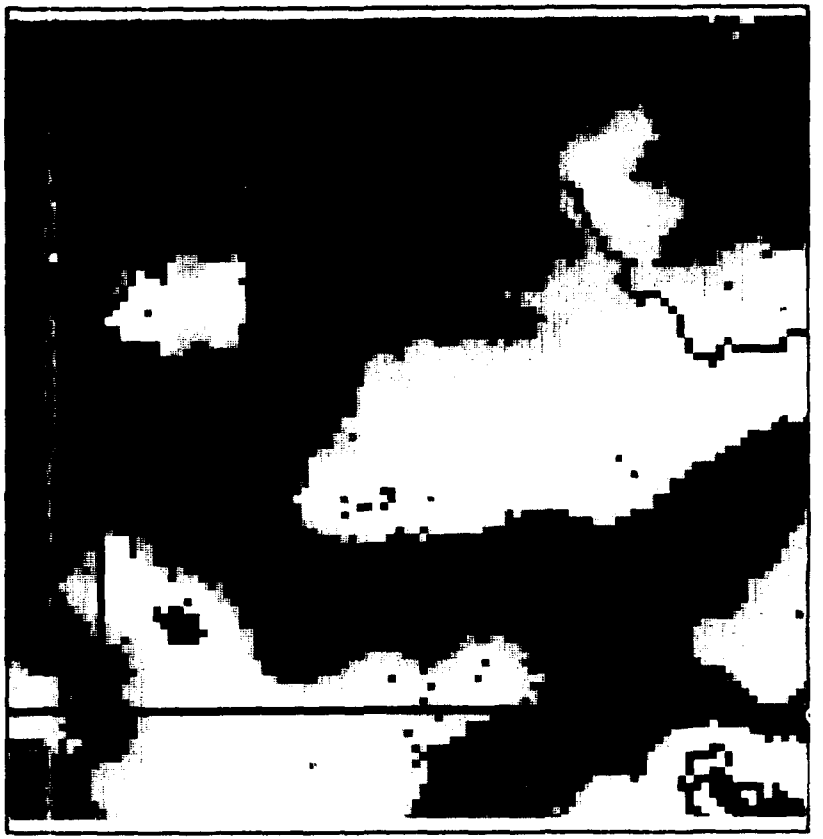

Figure 4.28 - 26 February window one SSM/I composite subscene.

The matching classified SSM/I subscene, figure 4.28, has a remarkably similar snow pattern as the AVHRR image. The shape and extent of snow cover along the Nevada and Idaho border is nearly an exact match of the snow found at the same location in the classified AVHRR scene. Similar snow patterns are also seen north of the Snake River Plain extending into Montana and along the eastern Idaho and Wyoming border. Snow is correctly imaged to the northeast of the Great Salt Lake but is once again erroneously depicted to the west of the lake in the salt flats. Snow is not observed in the SSM/I image in central and northern Idaho nor is it imaged in northeastern Oregon although it is seen in the AVHRR composite image. The strong snow signals (white) seen in the SSM/I image do match snow locations in the AVHRR image along the Idaho and Montana and Oregon borders. The snow not imaged in the SSM/I subscene depicted in the AVHRR scene may have too small an areal footprint to be imaged in the microwave channels or it may be of insufficient depth to be detected. The snow pack may also be in a particular physical state, such as refrozen snow, so that its brightness temperature is sufficiently warm to be separated as snow free land by the algorithm.

Figures 4.29 and 4.30 are the classified AVHRR and SSM/I images that correspond to figure 4.26, the channel 1 view of the window 2 subscene. The time of the SSM/I pass imaged in figure 4.30 is the same as that of figure 4.28. Figure 4.29 shows extensive cloud cover not readily observed in the channel AVHRR subscene. A large area of this cloud cover fails to get classified by the algorithm as was true in the window one subscene previously described. The weather depiction chart supports the existence of these clouds and the channel 1 image indicates that much of this cover is very thin. Much thicker cloud cover can be seen over the Sierra Nevada Range and also in southwestern Nevada. Significantly less snow appears in the Sierra Nevada Mountains compared with

Figure 4.29 - 26 February window two AVHRR composite subscene.

Figure 4.30 - 26 February window two SSM/I composite subscene.

that depicted in figure 4.23 of Case 4. More snow is found to the east in central and northern Nevada through gaps in the cloud cover than 12 days earlier.

The matching SSM/I image, figure 4.30, shows a very small extent of snow in the Sierra Nevada Range and practically no snow in Nevada. The snow in the mountains does appear to be in agreement with the AVHRR image but the lack of snow in the central part of the Nevada in the SSM/I image is disappointing. As discussed earlier, this snow is not exhibiting characteristics in agreement with the separation algorithm. Some of this snow was subject to the same melting conditions seen in Idaho as nearly all the reporting stations in Nevada reported temperatures above 50 degrees Fahrenheit at 2100 GMT, seven hours prior to the SSM/I pass. The foot print size of the microwave imagery may be too large to detect snow that is found located in relatively small areal concentrations such as mountain tops where the snow would tend to linger during melt off.

3. *Case 6*

Case 6 covers the same geographic locations as case four on 15 March, 1990. Figures 4.31 and 4.32 show the channel 1 AVHRR images for the window one and window two subscenes respectively. The time of the window one pass was 2126 GMT while the window two pass was at 2125 GMT. Isolated snow and snow showers had fallen in California, Idaho, Montana, Utah and Nevada for four days prior to this satellite pass. The 1900 GMT weather depiction chart on 15 March shows scattered to broken clouds at 4,000 to 7,000 feet AGL in southern Idaho and clear to scattered cloud decks at 4,000 to 5,000 feet AGL across Nevada and into Utah.

Figures 4.33 and 4.34 are the AVHRR and SSM/I classified composite images that correspond to the AVHRR channel 1 Idaho subscene, figure 4.31. The SSM/I pass was at 04:16 GMT on 15 March, approximately 17 hours prior to the AVHRR imagery.

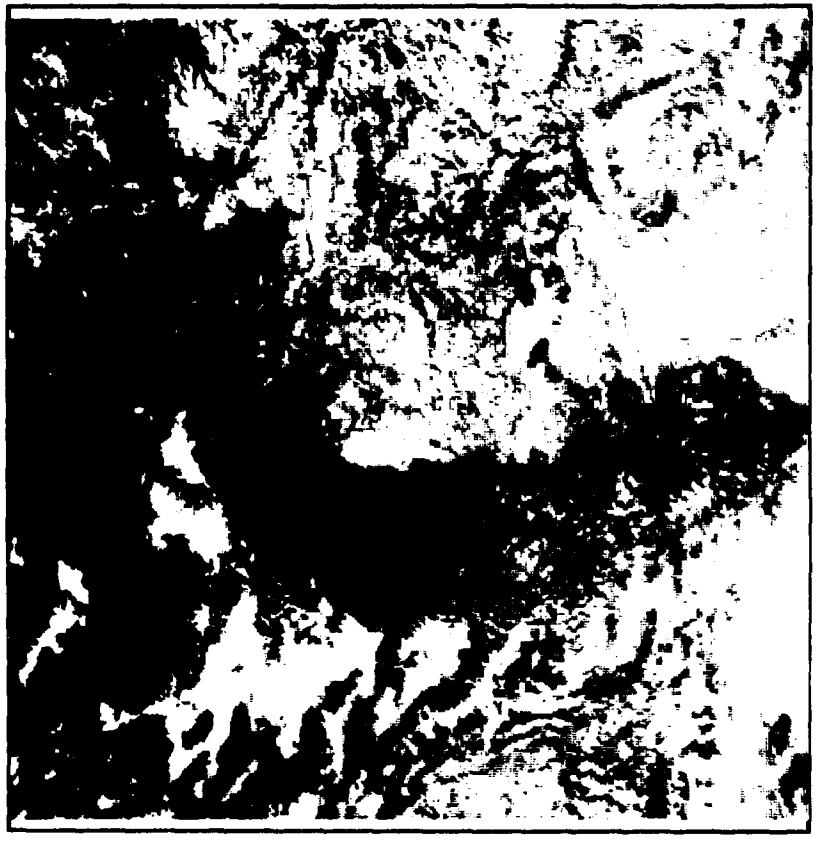

Figure 4.31 - 15 March AVHRR channel 1 window one subscene.

Figure 4.32 - 15 March AVHRR channel 1 window two subscene.

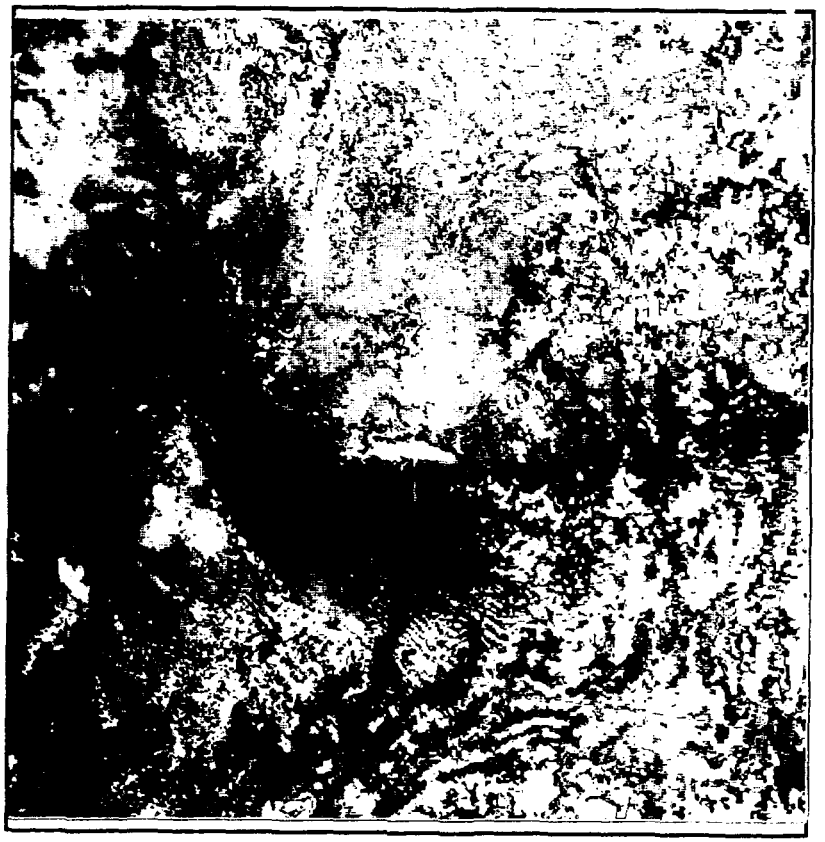

Figure 4.33 - 15 March window one AVHRR composite subscene.

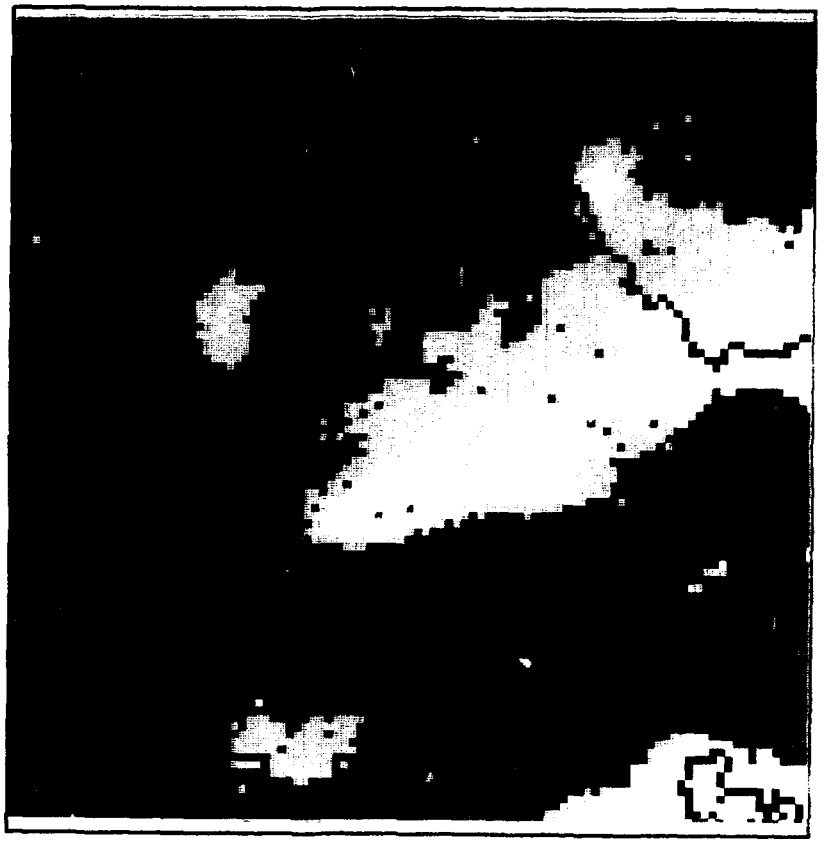

Figure 4.34 - 15 March window one SSM/I composite subscene.

The AVHRR classified composite image, figure 4.33, shows snow along the northern and southern side of the Snake River Valley underneath regions of broken clouds. Clouds (yellow) almost completely obscure the Great Salt and Bear Lakes. Compared to cases four and five, less snow is seen to the south of the valley along the Nevada and Idaho border. The snow line along the northern rim of the valley, particularly to the northwest near Boise, is more jagged and less distinct.

The classified matching SSM/I image, figure 4.34, also indicated less snow than seen in previous cases. Very little snow is analyzed along the southern side of the Snake River Valley and the outline of the valley has nearly been lost. Some snow is depicted along the Idaho and Nevada border and, although smaller in areal extent, this snow compares well with the AVHRR image. Snow is also found along the northern rim of the valley extending to the northeast into Montana as is also depicted in figure 4.33. Unlike the AVHRR subscene only one pixel of snow is shown in Oregon. Snow is again depicted in the vicinity of west of Great Salt Lake in the SSM/I image and is not seen in AVHRR image.

Analysis of the algorithm shows that snow is detected in all frequency combinations west of the Great Salt Lake except in the 85 minus 37 GHz horizontally polarized brightness temperature difference. This indicates that the shorter wavelengths are not scattered more than the longer wavelengths in this area. The false snow signal may be a result of the molecular structure of the salt flats, which might result in a lower emissivity than that found in other snow free land. The 37 GHz polarization difference is positive to strongly positive, indicating the presence of snow to open water in the algorithm respectively. There may be areas of standing water in the salt flats as wells as regions of the flats that are saturated with moisture. The physical characteristics of this region cause the algorithm to repeatedly misinterpret these pixels as a strong snow signal.

Figure 4.35 and 4.36 are the respective AVHRR and SSM/I classified composite images that correspond to the window two subscene shown in AVHRR channel 1 as figure 4.32. Snow in the Sierra Nevada Range covers a larger area than seen in case five, clearly extending from north to south across the entire subscene. Excellent separation of the mountain lakes is again depicted in this image. A large area of unclassified pixels extends in the lee of the Sierra Nevada Mountain Range and is likely caused by very thin cirrus that is not imaged in the channel 1 subscene. These clouds are either too warm to satisfy the channel 4 threshold for high clouds or too thin to be represented as a distinct cloud surface. Snow can be seen in central Nevada at higher elevations in both the classified and channel 1 AVHRR images.

The matching SSM/I image, figure 4.36, shows less coverage of snow in the Sierra Nevada Range than seen in the AVHRR images. Almost all of this snow is depicted south of Lake Tahoe. Snow is also depicted in Nevada just northeast of Lake Tahoe but may be caused by Pyramid Lake and not snow. No snow is imaged in central Nevada as was depicted in the AVHRR subscenes. Again, the thresholds necessary to separate pixels as snow in the algorithm have not been satisfied. Specifically, the snow is too thin to create the differential scattering necessary for the brightness temperature or polarization differences to be detected and the single brightness temperature thresholds required for weak snow are not met.

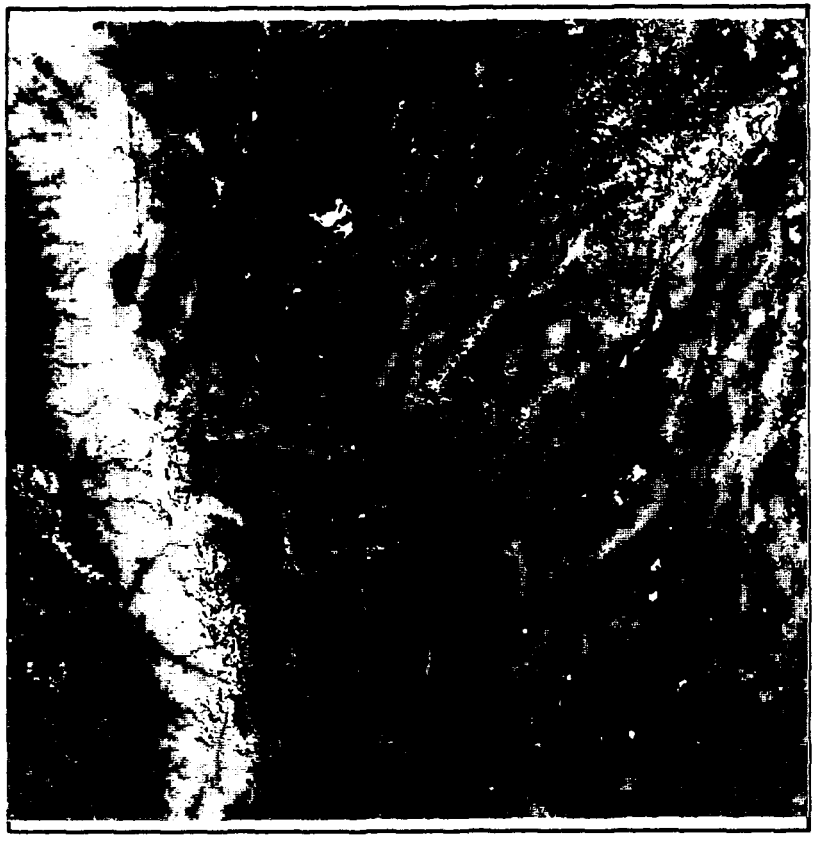

Figure 4.35 - 15 March window two AVHRR composite subscene.

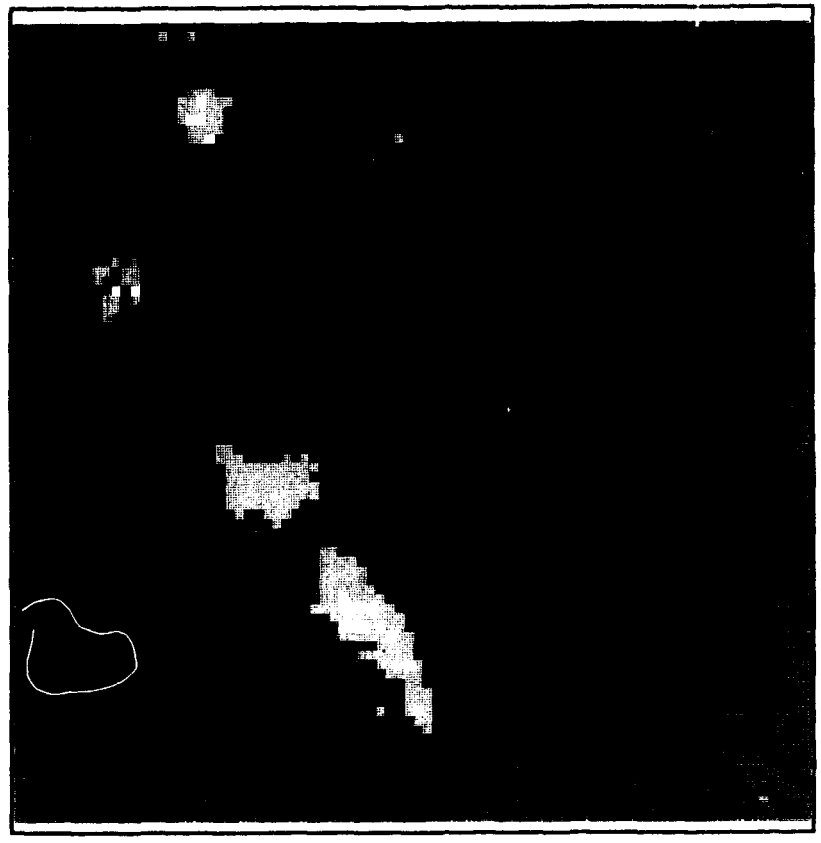

Figure 4.36 - 15 March window two SSM/I composite subscene.

V. SUMMARY AND RECOMMENDATIONS

Two image separation algorithms have been developed; one to classify AVHRR images given channels 1 through 4 data and the other to classify SSM/I images given the 37 GHz horizontal and vertical channels and the 85 GHz horizontal data. These algorithms were constructed by empirically determining the emission thresholds of each surface through the use of scatterplots. These thresholds were then set in an ordered series of FORTRAN block-if statements that separated the image. An entirely new, classified composite image was created by each algorithm where every surface of interest was shaded as a distinct gray shade. The algorithms were developed and tested from six subscenes taken from 1990 AVHRR and SSM/I data over the Great Lakes and then further tested and modified from six additional subscenes taken from mountainous regions of the western United States.

The AVHRR classification algorithm produced credible results. The initial program, created using AVHRR data from the Great Lakes, required modification for the western AVHRR data. Specifically, the reflectance values of snow free land had to be raised to correctly classify desert type sand which had significantly higher albedo than snow free land found in the Great Lakes region. Additionally, the channel 4 brightness temperature threshold for high clouds had to be lowered so that cold mountain tops were not classified as cloud. After the algorithm was modified all of the Great Lakes cases were run again so that a single algorithm was used for every case study. The changes made to improve the algorithm for the western data caused no significant changes in the Great Lakes classified scenes.

The algorithm was successful in separating snow from land pixels, making the snow line of the AVHRR scenes distinct. Especially impressive in the algorithm was the strong and accurate determination of lakes and waterways. This had been a problem early in the development of the algorithm. The low albedos of land and water made distinction of these two surfaces difficult and land pixels were often erroneously placed in lake locations. The use of a positive channel 2 minus channel 1 reflectance difference, unique to land surfaces, made separation possible. In several images, the classification of water pixels was believed to include melting snow. Liquid clouds, set apart by a large channel 3 minus channel 4 brightness temperature difference, also were strongly segregated in the algorithm. At times this separation appeared to be too severe, making the cloud fields in the classified image slightly more extensive than seen in the channel 1 image. Higher clouds, separated with a single channel 4 brightness temperature threshold, were subject to missed classification, or in the case of the western data, no classification at all. While the unclassified pixels (red) certainly indicated the likely presence of clouds in these data sets, the use of a single threshold in a classification routine is subject to error unless this single threshold will be intentionally varied from scene to scene to fit local conditions.

In summary, the AVHRR classification routine performed well over a significantly large time span in a variety of locations with largely varying topography and surface albedos. Except for the accurate segregation of higher ice type clouds, the algorithm appeared to be very stable. A great deal of confidence was placed in the result of the algorithm output to accurately detect snow and serve as a benchmark for comparison of the SSM/I classified images. The strength of the AVHRR classification routine lies in the fact that AVHRR data consists of four different channels of high resolution data that are equal in footprint size and permit direct comparison. These different channels allow for

the contrast of reflectance and brightness temperatures to be used to multi-spectrally identify major surfaces in the image.

Successful viewing of the snow pack with AVHRR imagery is totally dependent on cloud conditions at the time of the satellite pass and can only be accomplished during daylight hours. This can be a severe restraint during the winter season when inclement weather can persist for days. A great deal of information can be lost about the snow pack during cloud covered days when rapid changes in the snow depth and extent can occur due to additional snow accumulation or melt off.

SSM/I imagery offers the promise of viewing the snow fields without cloud contamination, day or night. The SSM/I algorithm was also successful in identifying snow fields using a combination of the 37 GHz vertical and horizontal channels as well as the 85 GHz horizontal channel. Major snow covered areas were practically visible in the unclassified 85 GHz horizontal image and were best separated in the algorithm by examining the differences of the 85 GHz horizontal channel minus the 37 GHz horizontal channel or the 37 GHz vertical and horizontal polarization difference. During algorithm development, these techniques produced very similar results so both methods were incorporated in to the separation algorithm.

Additional steps to attempt to identify weaker snow signals were empirically obtained and added to the algorithm. These steps assigned high and low brightness temperatures for each channel to form a bi-spectral box which a given pixel needed to fit through to be classified. Unlike the 85 GHz minus the 37 GHz horizontal brightness temperature difference or the 37 GHz polarization difference, the non differenced thresholds were more sensitive to variation in surface temperature due to changes in microwave emission. As with the AVHRR separation algorithm, thresholds formed from channel differencing

were much more stable than those derived from high and low values taken from single channels and were more useful in a universal algorithm.

Unequal footprint sizes of the 85 GHz and 37 GHz microwave channels and the single parameter output of brightness temperature make the SSM/I algorithm much less sophisticated than the AVHRR routine. There is simply less information about a particular location that is available to determine the pixel identity. The addition of more channels, such as the 19 GHz or 22 GHz channel, creates a more complete data base at the expense of lost resolution. The SSM/I composite images created in this study are very coarse compared to the AVHRR result but very large sections of the country are covered in a single pass. Additionally, the surface of the earth remains visible in the presence of non-precipitating clouds.

The comparative AVHRR and SSM/I composite images exhibited similar snow patterns and areal extent of snow. Agreement was found with the strong snow SSM/I signal and the overall snow depicted in the AVHRR image. That is, the strong snow SSM/I signal normally fell within the snow edges found in the AVHRR composite images. In general the SSM/I imagery showed a smaller areal extent of snow cover than the AVHRR composite image. This is likely due to the thresholds set for the weaker snow category in the SSM/I algorithm which appeared to be sensitive to local temperature variation. It was also due to the fact that the different footprint sizes of the two images require different sized physical areas of snow extent before a pixel could be considered to be snow covered. Additionally, this research seems to confirm that there is a critical snow depth that must be reached before the volume scattering difference between the 85 GHz horizontal and 37 GHz horizontal channels or the 37 GHz vertical and 37 GHz horizontal channels can be noticed.

In both algorithms it appeared that snow detection performance was best over flat terrain as compared to mountainous terrain. Shadowing and temperature variations have been noted to degrade the AVHRR algorithm performance. In the SSM/I case it is believed that the temperature variations also cause variations in the surface emission. Further, the chances of a photon leaving a flat, planar surface and reaching the satellite sensor seem much better than one exiting an oblique surface, such as a mountain side facing away from the sensor.

The following comments are offered as improvements that could be made to this study during further research:

1. Investigate the SSM/I 85 GHz polarization difference using data that contains both the 85 GHz horizontally and vertically polarized channels. The resolution seen in the 85 GHz channels is far superior to the 37 GHz channels and may be able to detect the snow edge in a manner similar to the 37 GHz polarization scheme referenced and used in this study.

2. Consider the use of manipulated algorithms that would ingest a local set of surface observations to finely tune the thresholds used to determine surface separation. This type of algorithm, although more cumbersome than a universal routine, might prevent some of the problems encountered with single channel, undifferenced thresholds. The data is readily available, and might be fed into the algorithm without a significant loss of processing time.

3. Rerun the experiment conducted by McFarland *et al.* (1987) with SSM/I data. A new field experiment is needed to understand the behavior of the snow pack in the higher resolution microwave channels. Studies of snow depths needed to trigger bi-spectral differential scattering, as well as the areal extent of snow coverage necessary for pixel classification in a designated algorithm would give the remotely sensed data more credibility. Actual ground truth and aircraft survey should be conducted at the time of satellite sampling to monitor snow pack extent, snow water equivalent and physical snow condition. This would empirically give insight to the behavior of the satellite data. AVHRR data should be simultaneously collected over the same test locations for comparison during favorable weather conditions.

4. Set up operational SSM/I windows that match active AVHRR snow windows and receive this data in as near a real time format as possible. Map the two data sets using the same projection. Use the AVHRR data to calibrate the SSM/I data when weather conditions permit and then follow the snow line with the SSM/I imagery during inclement weather throughout a winter season.

The AVHRR imagery taken from CD-ROM used in this thesis consists of high resolution data in four channels that can be used to determine the areal extent of snow cover. Given clear atmospheric conditions, it is definitely the first choice data for this type of environmental observation. SSM/I imagery offers large areal coverage of the ground in nearly all weather conditions, day or night. While daily coverage is not necessarily available below 50 degrees latitude, this study noted that coverage of a given area of the United States was accomplished every 2 to 3 days with overlap. Even though the resolution of the SSM/I data is poor compared to the AVHRR imagery, these data are useful. It can certainly augment information provided by AVHRR imagery at this time. Continued improvements in the algorithms and better understanding of the physical mechanisms that alter the microwave signature of the snow pack and surrounding terrain will increase the usefulness of SSM/I data in the future.

REFERENCES

Allen, R.C., Jr. , 1987: Automated satellite cloud analysis: A multispectral approach to problem of snow cloud discrimination. M.S. Thesis, Naval Postgraduate School, Monterey, CA, June 1987.

Allen, R.C., Jr., Durkee P.A., and C.H. Wash, 1990: Snow/cloud discrimination with multispectral satellite measurements. *J. Appl. Meteor.*, **29**, 994-1004.

Barron, J.P., 1988: An objective technique for Arctic cloud analysis using mutispectral AVHRR satellite imagery. M.S. Thesis, Naval Postgraduate School, Monterey, CA, March, 1988.

Carroll, T.R., 1990: Operational airborne and satellite snow cover products of the National Operational Hydrologic Remote Sensing Center, p.97. Proceedings of the Forty-Seventh Annual Eastern Snow Conference. CRREL Special Report 90-44.

Ferraro, R.R., Jr., Grody, N.C., and J.A. Kogut, 1986: Classification of geophysical parameters using microwave satellite measurements, *IEEE Trans. Geosci. Remote Sensing*, **GE-24**, 1008-1013.

Kong, J.A., Shin, R., Shiue, J.C., and L. Tsang, 1979: Theory and experiment for passive microwave remote sensing of snowpacks, *J. Geophys. Res.*, **84**, 5669-5673.

Kunzi, K.F., Patil, S., and H. Rott, 1982: Snow-cover parameters retrieved from Nimbus-7 Scanning Multichannel Microwave Radiometer (SMMR) Data, *IEEE Trans. Geosci. Remote Sensing*, **GE-20**, 452-467.

McFarland, M.J., Wilke, G.D., and P.H. Harder,II, 1987: Nimbus 7 SSMR investigation of snowpack properties in the northern Great Plains for the winter of 1978-1979, *IEEE Trans. Geosci. Remote Sensing*, **GE-25**, 35-46.

National Operational Hydrologic Remote Sencing Center, CD-ROM Users Guide, 1990: 1990 Airborne and Satellite Snow Data CD-ROM, Office of Hydrology, NWS, NOAA, 6301-34th Avenue South, Minneapolis, Minnesota 55450-2985.

Spenser, R.W., Goodman, H.M., and R.E. Hood, 1988: Precipitation retrieval over land and ocean with the SSM/I: Identification and characteristics of the scattering signal, *J. Atmos. Ocean. Tech.*, **6**, p. 255.

Srivastav, S.K, and R.P Singh, 1991: Microwave radiometry of snow covered terrains, *Int. J. Remote Sensing*, **12**, 2117-2131.

APPENDIX A

REPRESENTATIVE AVHRR SCATTERPLOTS

This appendix contains one set of representative scatterplots used to select thresholds for the AVHRR separation algorithm. Different channel combinations were plotted in an overall 512 x 512 scene, using only every 16th data point to reduce the total number of point combinations plotted. Specific surfaces, such as snow free land or cumulus clouds were then selectively sampled in 40x40 pixel blocks and scatterplotted. The labeled shapes drawn on the plots in this section indicate the regions that the selected surfaces occupy. The abbreviations used on the plots are interpreted as follows:

- Ci - cirrus (high) cloud
- Cu - cumulus (liquid) cloud
- LD - snow free land
- LK - lake
- S:HR - high reflectance snow
- S:LR - low reflectance snow

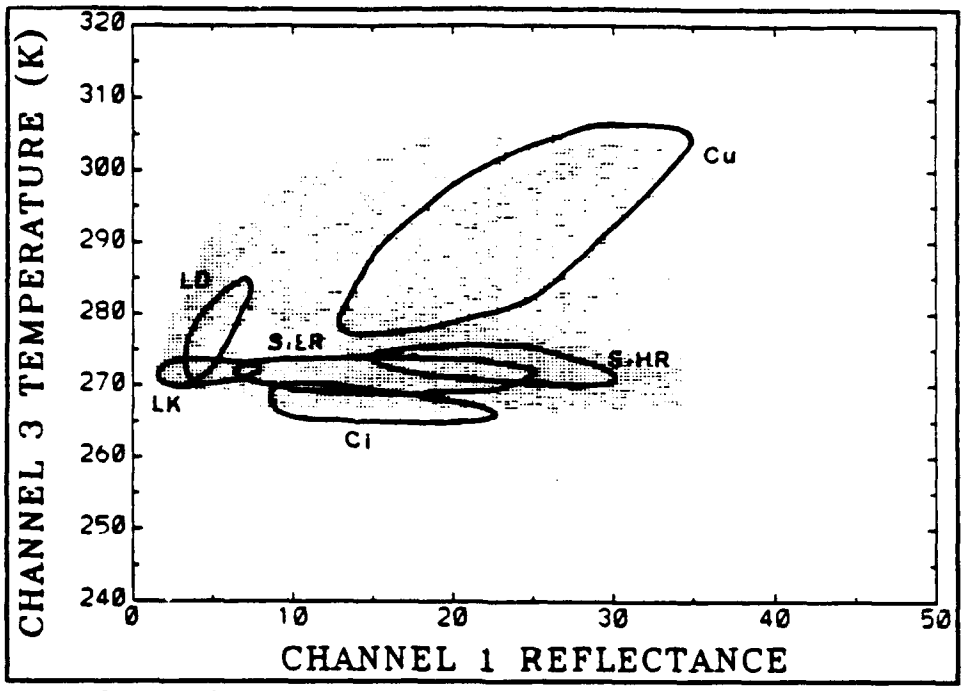

Figure A.1 - Channel 3 versus channel 1 scatterplot of west Great Lakes subscene on 20 February 1990. Brightness temperature in degrees K, reflectance in scaled albedo.

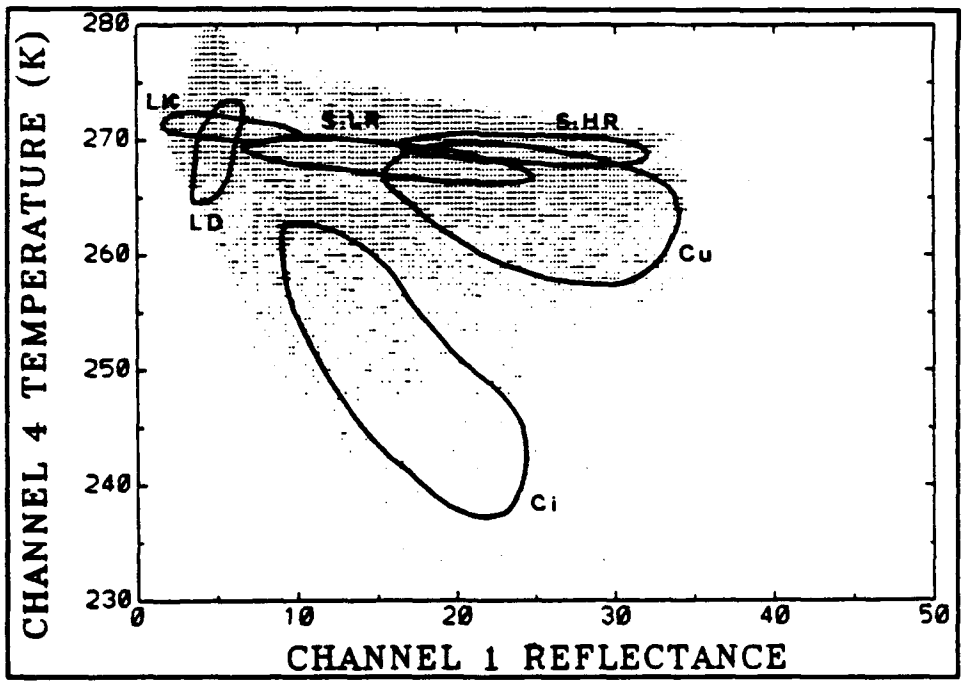

Figure A.2 - Channel 4 versus channel 1 scatterplot of west Great Lakes subscene on 20 February 1990. Brightness temperature in degrees K, reflectance in scaled albedo.

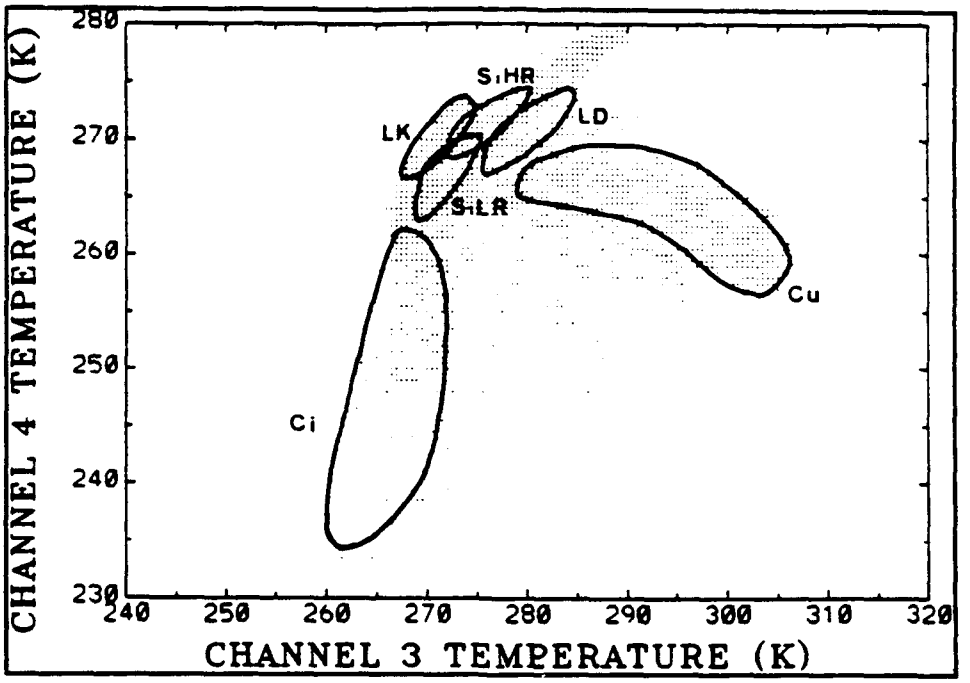

Figure A.3 - Channel 4 versus channel 3 scatterplot of west Great Lakes subscene on 20 February 1990. Brightness temperature expressed in degrees K.

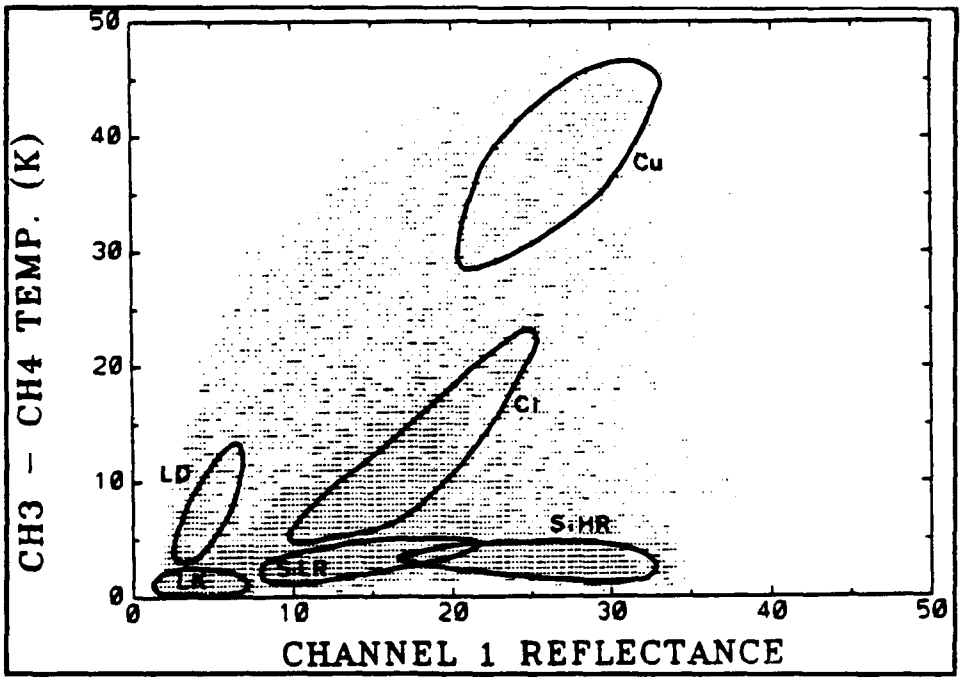

Figure A.4 - Channel 3 minus channel 4 versus channel 1 scatterplot of west Great Lakes subscene on 20 February 1990. Brightness temperature expressed in degrees K, reflectance in scaled albedo.

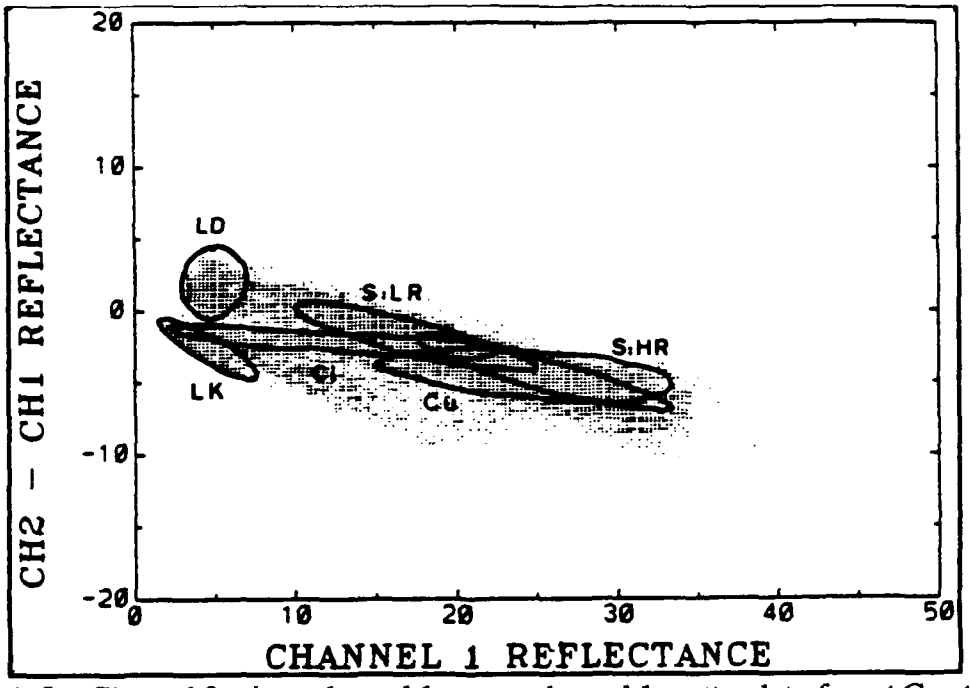

Figure A.5 - Channel 2 minus channel 1 versus channel 1 scatterplot of west Great Lakes subscene on 20 February 1990. Reflectance expressed in scaled albedo.

APPENDIX B

REPRESENTATIVE SSM/I SCATTERPLOTS

This appendix contains one set of representative scatterplots used to select thresholds for the SSM/I separation algorithm. Different channel combinations were plotted in an overall 512 x 512 scene, using only every fourth data point to reduce the total number of point combinations plotted. Specific surfaces, such as snow free land or snow were then selectively sampled in 30x30 pixel blocks and scatterplotted. The labeled shapes drawn on the plots in this section indicate the regions that the selected surfaces occupy. The abbreviations used on the plots are interpreted as follows:

- LD - snow free land
- LK - lake
- SS - strong snow signature
- WS - weak snow signature

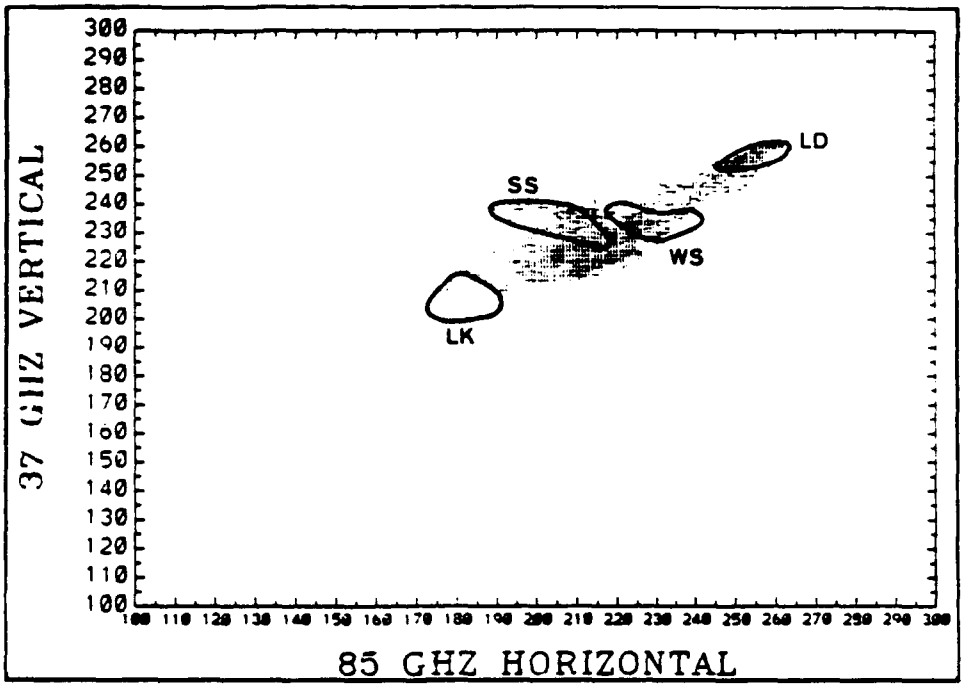

Figure B.1 - 37 GHz vertical versus 85 GHz horizontal scatterplot of west Great Lakes subscene on 20 February 1990. Brightness temperature in degrees K.

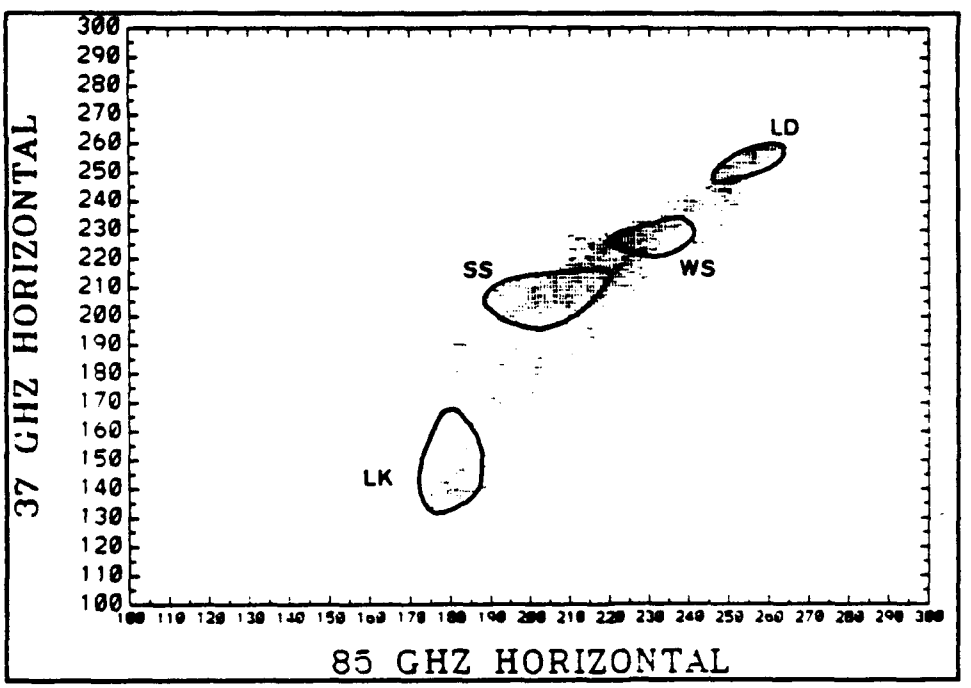

Figure B.2 - 37 GHz horizontal versus 85 GHz horizontal scatterplot of west Great Lakes subscene on 20 February 1990. Brightness temperature in degrees K.

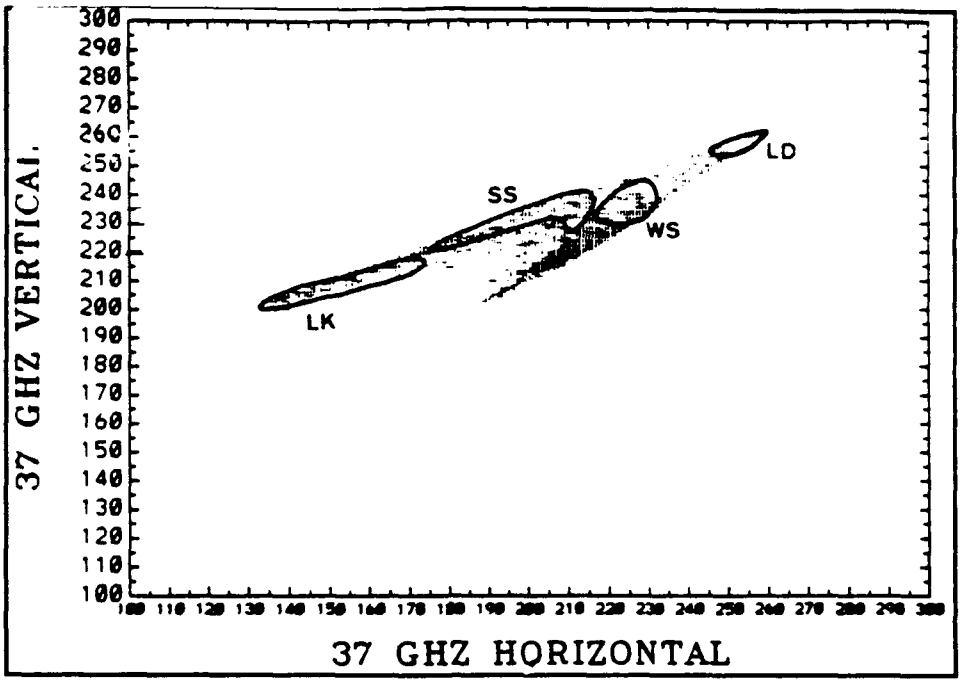

Figure B.3 - 37 GHz vertical versus 37 GHz horizontal scatterplot of west Great Lakes subscene on 20 February 1990. Brightness temperature expressed in degrees K.

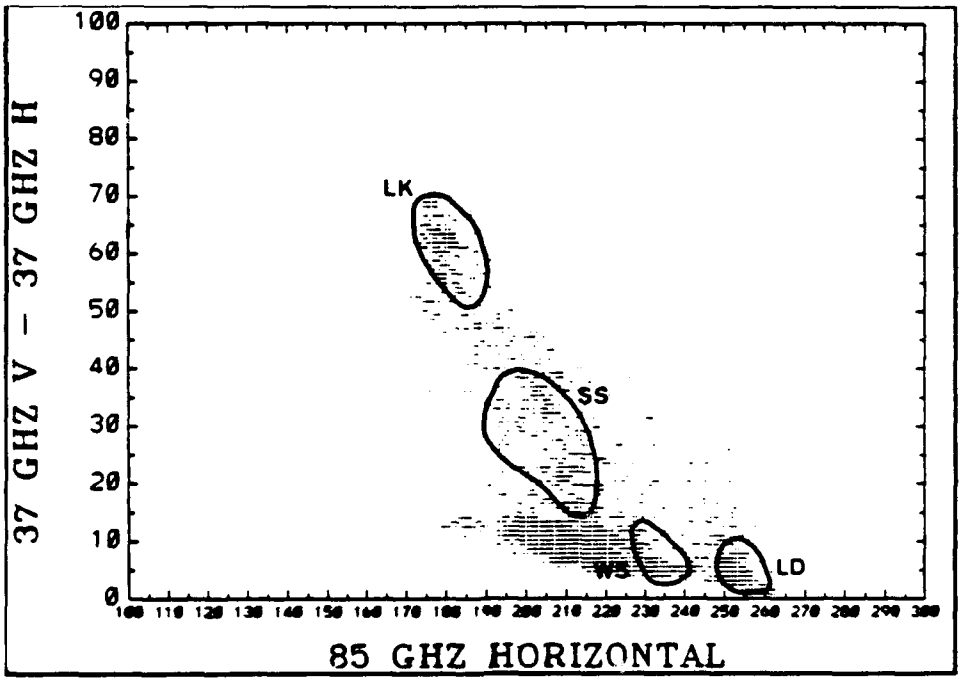

Figure B.4 - 37 GHz vertical minus 37 GHz horizontal versus 85 GHz horizontal scatterplot of west Great Lakes subscene on 20 February 1990. Brightness temperature expressed in degrees K.

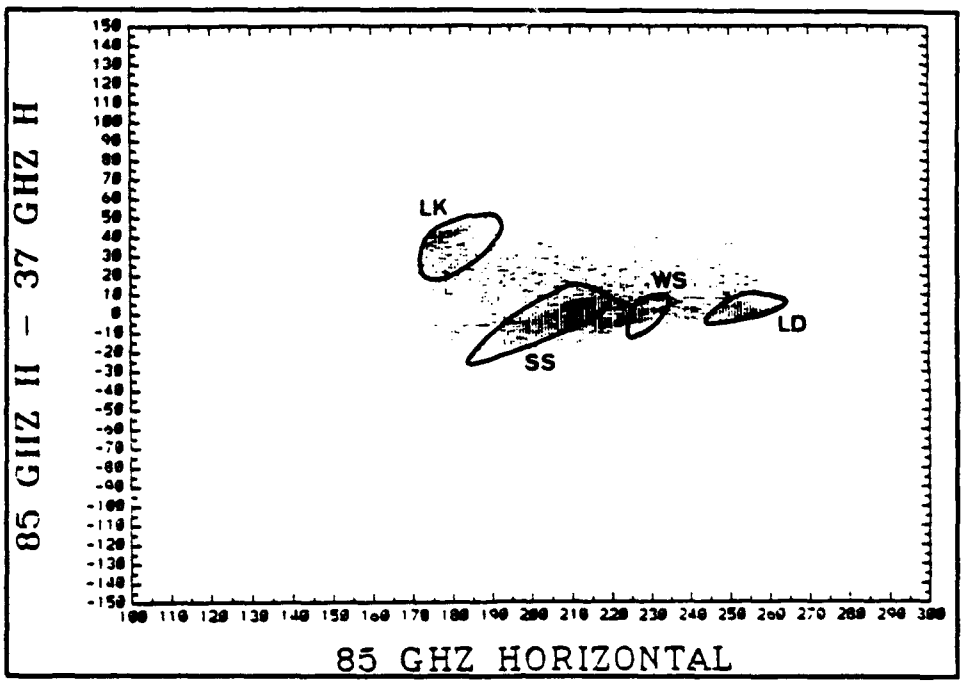

Figure B.5 - 85 GHz horizontal minus 37 GHz horizontal versus 85 GHz horizontal scatterplot of west Great Lakes subscene on 20 February 1990. Brightness temperature expressed in degrees K.

INITIAL DISTRIBUTION LIST

1.	Defense Technical Information Center Cameron Station Alexandria, VA 22304-6145	2
2.	Library, Code 52 Naval Postgraduate School Monterey, CA 93943-5000	2
3.	Chairman (Code OC/Co) Department of Oceanography Naval Postgraduate School Monterey, CA 93943-5000	1
4.	Chairman (Code MR/Hy) Department of Meteorology Naval Postgraduate School Monterey, CA 93943-5000	1
5.	Professor P.A. Durkee Department of Meteorology (Code MR/De) Naval Postgraduate School Monterey, CA 93943-5000	2
6.	Professor C.H. Wash (Code MR/Wx) Department of Meteorology Naval Postgraduate School Monterey, CA 93943-5000	1
7.	Lieutenant Commander R.W. Maxson, NOAA Deputy Director NWS/NOHRSC W/OH23 6301 34th Avenue South Minneapolis, MN 55450	2
8.	NOAA Corps Commissioned Personnel CPC-2 Rockville, MD 20852	1

9. Director, NOAA AOC 1
P.O. Box 020197
Miami, FL 33102-0197

10. Dr. T.R. Carroll, NOAA 1
Director, NWS/NOHRSC W/OH23
6301 34th Avenue South
Minneapolis, MN 55450

11. Dr. R.L. Armstrong 1
CIRES/NSIDC C.B. 449
University of Colorado
Boulder, CO 80309